JRC Scientific and Technical Reports

Temporal Variability of Ocean Colour Derived Products In the European Seas

V. Vantrepotte & F. Mélin

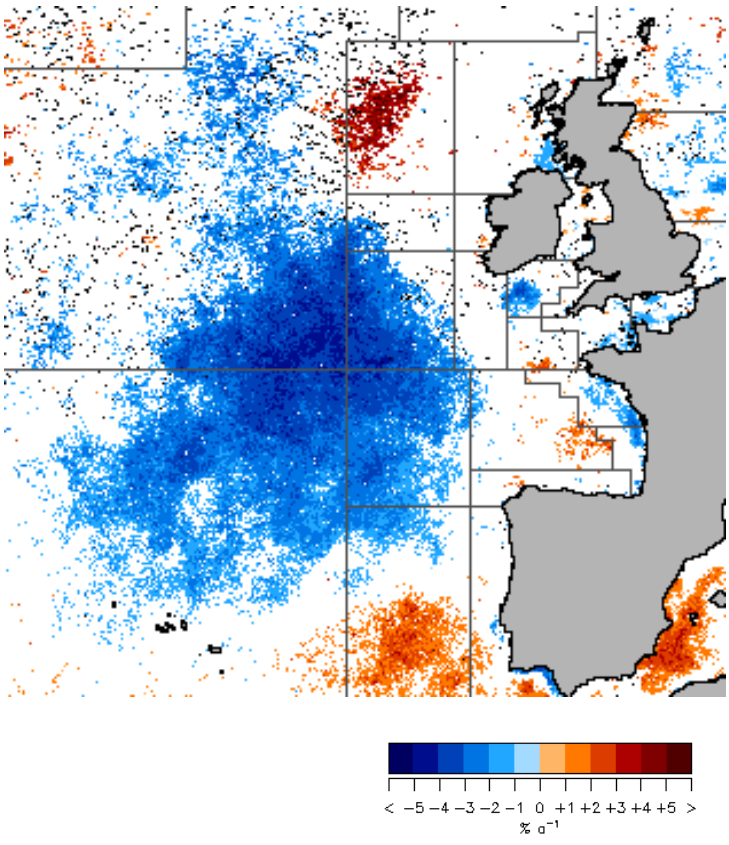

EUR 23579 EN - 2008

JRC EUROPEAN COMMISSION

ies Institute for Environment and Sustainability

The mission of the Institute for Environment and Sustainability is to provide scientific-technical support to the European Union's Policies for the protection and sustainable development of the European and global environment.

European Commission
Joint Research Centre
Institute for Environment and Sustainability

Contact information
Address: Frédéric Mélin, E.C. JRC, IES, GEM, via Fermi, 2749, Ispra, 21027, Italy
E-mail: frederic.melin@jrc.it
Tel.: +39 – 0332 - 8785627
Fax: +39 – 0332 - 789034

http://ies.jrc.ec.europa.eu/
http://www.jrc.ec.europa.eu/

JRC 48490

EUR 23579 EN

ISSN 1018-5593

Luxembourg: Office for Official Publications of the European Communities

Printed in Italy

Abstract

The ten-year record of ocean colour data provided by the SeaWiFS mission is an important asset for monitoring and research activities conducted on the optically-complex European seas. This study mainly makes use of the SeaWiFS data set of normalized water leaving radiances L_{WN} to study the major characteristics of temporal variability associated with optical properties across the entire European domain. Specifically, the time series of L_{WN}, band ratios, diffuse attenuation coefficient $K_d(490)$ and concentration of chlorophyll *a* Chl*a* are decomposed into terms representing a fixed seasonal cycle, irregular variations and trends, and the contribution of these components to the total variance is described for the various basins. The diversity of the European waters is fully reflected by the range of results varying with regions and wavelengths. Generally, the Mediterranean and Baltic seas appear as two end-members with, respectively, high and low contributions of the seasonal component to the total variance. The existence of linear trends affecting the satellite products is also explored for each basin. The interpretation of the trends observed for L_{WN} and band ratios is not straightforward, but it circumvents the limitations resulting from the levels of uncertainty, very variable in space and often high, that characterize derived products such as Chl*a* in European waters. Results for $K_d(490)$ and Chl*a* are also analyzed. Statistically significant, and in some cases large, trends are detected in the Atlantic Ocean west of the European western shelf, the central North Sea, the English Channel, the Black Sea, the northern Adriatic, and various regions of the Mediterranean Sea and the northern Baltic Sea, revealing changes in the concentrations of optically significant constituents in these regions.

Contents

Introduction

Optical remote sensing (ocean colour) is a valuable source of information on marine ecosystems as it provides quantitative estimates of the optical properties associated with seawater. These are associated with the concentrations of optically significant constituents, a major example being the concentration of the pigment chlorophyll *a* (Chl*a*) that can be considered as a proxy for algal biomass. Other variables that can be quantified by bio-optical algorithms include the absorption by chromophoric dissolved organic matter (CDOM), and the concentration of total suspended matter (TSM). Additionally, optical properties per se are indicators of the status of marine ecosystems and can be used to derive characteristics such as turbidity or transparency.

The European seas encompass a wide range of water types (Berthon et al., 2008), including oligotrophic regions, phytoplankton-rich upwelling zones, and scattering or absorbing waters, typically in the North or Baltic Seas, a diversity that reflects the characteristics of the local systems. In fact, the European seas offer numerous examples of optically complex water bodies, as several factors interact to drive their optical signature, including biological activity (production and degradation of organic matter), inputs from the coastline and river outflows, and particle re-suspensions from the bottom. The prevalence of continental, often relatively absorbing, aerosols, and the existence of shallow areas (with their possible effect on the light field) are other factors making a consistent quantitative use of ocean color remote sensing at the scale of the European seas a challenging task. Logically high uncertainties related with standard ocean colour products like Chl*a* have been documented for European waters (e.g., Darecki and Stramski, 2004 for the Baltic; Blondeau-Patissier et al., 2004; McKee et al., 2007 for North, Irish and Celtic Seas; Sancak et al., 2005, Oguz and Ediger, 2006, for the Black Sea; Mélin et al., 2007; Volpe et al., 2007 for the Mediterranean). These uncertainties have so far impeded the full integration of ocean colour remote sensing in monitoring strategies at the continental scale, even if advancements are noticeable for specific regions.

Simultaneously there is a dire need for an improved characterization of the European seas. Recent Communications from the European Commission to the Council and the European Parliament (COM, 2002 539; COM, 2005 504) have recognized that the status of the European marine domain, faced with various pressures and threats, has overall been deteriorating over the past decades, a situation prompting the establishment of "a framework for Community action in the field of marine environmental policy" (the upcoming Marine Strategy Framework Directive). The existing legislation for coastal waters (Directive 2000/60/EC) already specifically calls for the monitoring of various quality elements (including phytoplankton biomass and transparency) and the assessment of long-term changes in natural conditions.

In that context, the availability of a ten-year satellite record of optical properties represents an asset for a comprehensive and consistent assessment of major char-

acteristics of the European seas. The present work mainly focuses on the analysis of the temporal variability of apparent optical properties (AOPs), water leaving radiance and diffuse attenuation coefficient, at the European scale. Analyzes of temporal variability of the ocean color Chl$a$ record have been conducted at global or basin scales (e.g., Yoder and Kenelly, 2003; McClain et al., 2004) but in that respect AOPs have been comparatively ignored. Even though the interpretation of results dealing with AOPs is not necessarily as straightforward as with derived products like Chl$a$, that does not lessen the potential offered by these data sets. Conversely an advantage is to circumvent the obstacle represented by the level of uncertainties affecting bio-optical algorithms used to obtain European-scale derived products. Here standard products of chlorophyll a concentration are only considered for completeness and with due caution. The first objective of this study is to analyze the main temporal patterns associated with the various sub-regions of the European seas in terms of spectral AOPs and to classify them accordingly, therefore supporting an enhanced characterization of the essential features of European waters. An accompanying goal is to determine where trends in optical properties, and therefore in the content of the surface waters, can be detected with the present data records. The satellite data set, the partition of the European seas and the statistical approach used for the analysis are first presented. Then results are described and discussed at the level of separate basins and synthesized at the scale of the European marine domain.

This report corresponds to the final deliverable of the E.C. Joint Research Centre in the framework of WP3250 of the MARine and COASTal Environmental Information Services (MarCoast) - Water Quality Assessment Service - European Space Agency GMES Service Element.

Section 1

Data and Methods

1.1 Satellite Data

The satellite products are based on the imagery from the Sea-viewing Wide Field-of-view Sensor (SeaWiFS, Hooker et al., 1992). The satellite level-1A data have been acquired from the Goddard Space Flight Center (U.S. National Aeronautics and Space Administration) and processed with the SeaWiFS Data Analysis System (SeaDAS) software package version 5.1.5, that includes the updated calibration procedures associated with reprocessing 5.2. The analysis of temporal variability is based on Local Area Coverage (LAC) full-resolution imagery that is more suitable than Global Area Coverage (GAC) data for analyzes conducted in coastal waters. The resulting data set covers the domain 10°N-80°N, 40°W-55°E and the period includes seven years from November 1997 to October 2004 (December 2004 being the end of the unrestricted distribution of LAC data). A similar processing has been conducted using GAC data for the specific purpose of extending the computation of temporal trends over a 10-year period (November 1997 to October 2007), being well aware that the use of this record for small coastal regions needs caution.

The products hosted by the E.C. Joint Research Centre European archive (illustrated on http://oceancolour.jrc.ec.europa.eu) that are used in the present work include the normalized water leaving radiances L_{WN} at the center-wavelengths 412, 443, 490, 510, 555 and 670 nm, the diffuse attenuation coefficient K_d obtained at 490 nm by an empirical band-ratio algorithm (OBPG, Werdell, 2005) and the chlorophyll a concentration Chl$a$ derived from the standard global algorithm OC4v4 (O'Reilly et al., 2000). The atmospheric correction scheme is based on the work by Gordon and Wang (1994) and subsequent developments (e.g., Wang et al., 2005 and references therein). The L_{WN} values are corrected for bi-directional effects (according to Morel et al., 2002) and for out-of-band contributions (Wang et al., 2001). The processed imagery is then re-mapped on regular grids with a resolution of approximately 2 km and 9 km for LAC and GAC data, respectively. Finally, monthly composites are created using the daily maps.

The satellite L_{WN} data are expressed in radiance units, and are therefore proportional to the solar irradiance. It is thus worth recalling that a trend analysis related to L_{WN} over the last decade can be safely undertaken considering the temporal changes affecting the solar irradiance (typically less than 0.1% per decade; Willson and Mordvinov, 2003 and references therein).

1.2 Partition of the European Seas

The overall window is split into the major European basins as listed in Table 1.1.

Table 1.1: Definition of the four regions considered for analysis. Grid resolutions are approximately 2-km.

Notation	Description	Latitude	Longitude
BALT	Baltic Sea	52.75°N-66°N	3.5°E-30.5°E
BSEA	Black Sea	40.75°N-47.5°N	27.25°E-42°E
MEDI	Mediterranean Sea	30°N-46°N	6°W-36.5°E
NEAT	NE Atlantic	26°N-73.5°N	40°W-30.°E

Considering the complexity of describing the variability of spectral quantities over time and space, a data reduction is performed by considering a partition of the European waters. The definition of the regions are displayed on Fig. 1.1 to 1.4 with the corresponding acronyms for the four major domains:

1. the partition of the Mediterranean Sea (Fig. 1.1) reproduces that chosen by Bricaud et al. (2002), with a additional division of the Adriatic Sea,

2. the Black Sea provinces (Fig. 1.2) are defined on the basis of a division between western and eastern basins and bathymetry (200 m isobath, see for instance Kopelevich et al., 2002), with results computed for the western Black Sea shelf, the western deep Black Sea, the eastern deep Black Sea, and the Sea of Marmara,

3. the partition of the Baltic Sea (Fig. 1.3) is a synthesis of regions proposed by the International Council for the Exploration of the Sea (ICES), the Food and Agriculture Organization (region 27-IIId) and the Helsinki Commission (HELCOM), as well as common knowledge of the basin features,

4. the partition of the Northeast Atlantic is shown on Fig. 1.4, that follows the partition by ICES (FAO regions 27 and 34).

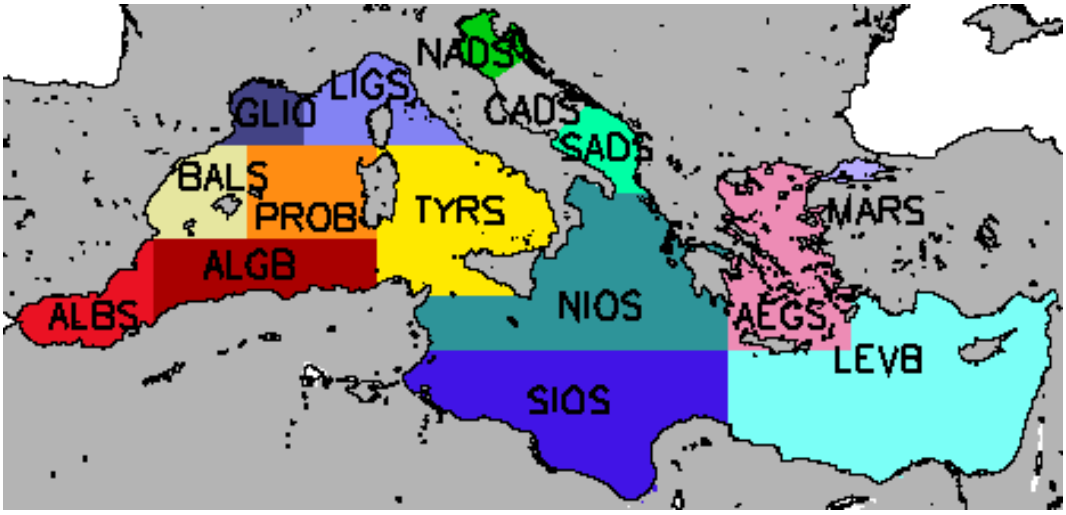

Figure 1.1: Partition of the Mediterranean Sea with: **ALBS**: Alboran Sea; **GLIO**: Gulf of Lions; **LIGS**: Ligurian Sea; **BALS**: Balearic Sea; **PROB**: Provencal Basin; **ALGB**: Algerian Basin; **TYRS**: Tyrrhenian Sea; **NADS**: Northern Adriatic Sea; **CADS**: Central Adriatic Sea; **SADS**: Southern Adriatic Sea; **NIOS**: North Ionian Sea; **SIOS**: South Ionian Sea; **AEGS**: Aegean Sea; **LEVB**: Levantine Basin; **MARS**: Marmara Sea.

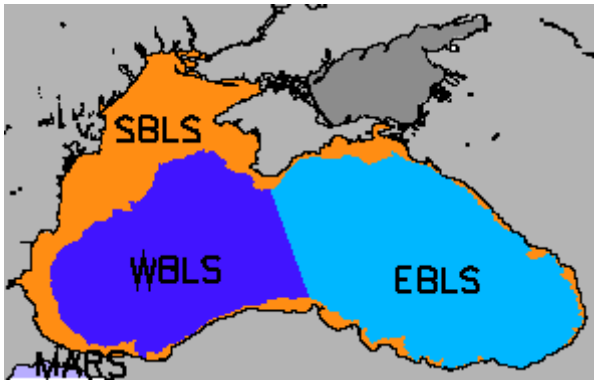

Figure 1.2: Partition of the Black Sea, with: **WBLS**: western deep Black Sea; **EBLS**: eastern deep Black Sea; **SBLS**: shelf Black Sea; **MARS**: Marmara Sea (see complete extent on Fig. 1).

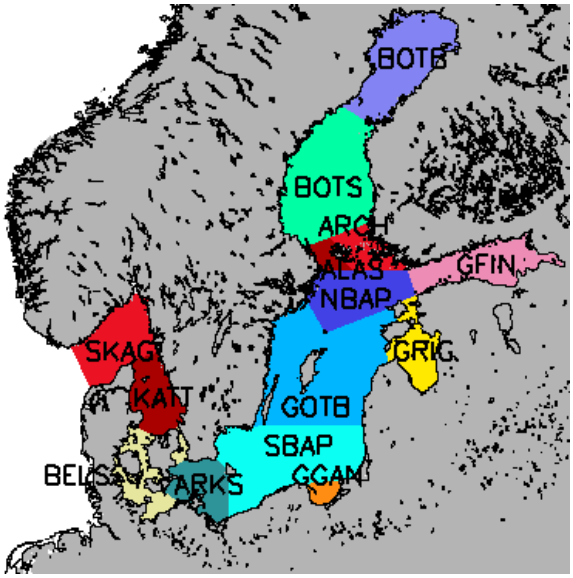

Figure 1.3: Partition of the Baltic Sea, with: **SKAG**: Skagerrak; **KATT**: Kattegat; **BELS**: Belt Sea; **ARKS**: Arkona Sea; **SBAP**: Southern Baltic Proper; **GGAN**: Gulf of Gdansk; **GOTB**: Gotland Basin; **GRIG**: Gulf of Riga; **NBAP**: Northern Baltic Proper; **GFIN**: Gulf of Finland; **ALAS**: Aland Sea; **ARCH**: Archipelago region; **BOTS**: Bothnian Sea; **BOTB**: Bothnian Bay.

For each province, average monthly time series are computed on the log-transformed data for normalized water leaving radiances $L_{WN}(\lambda)$, band ratios with respect to 555 nm $\rho(\lambda)$, the diffuse attenuation coefficient $K_d(490)$ and the concentration of chlorophyll *a* Chl*a*. Outliers (distant from the average value by more than $\pm$ 3 standard deviations) are excluded after one iteration. If the data available for a given month cover less than 10% of the surface area, the corresponding monthly average is discarded. The areal average data are then transformed back to the original scale.

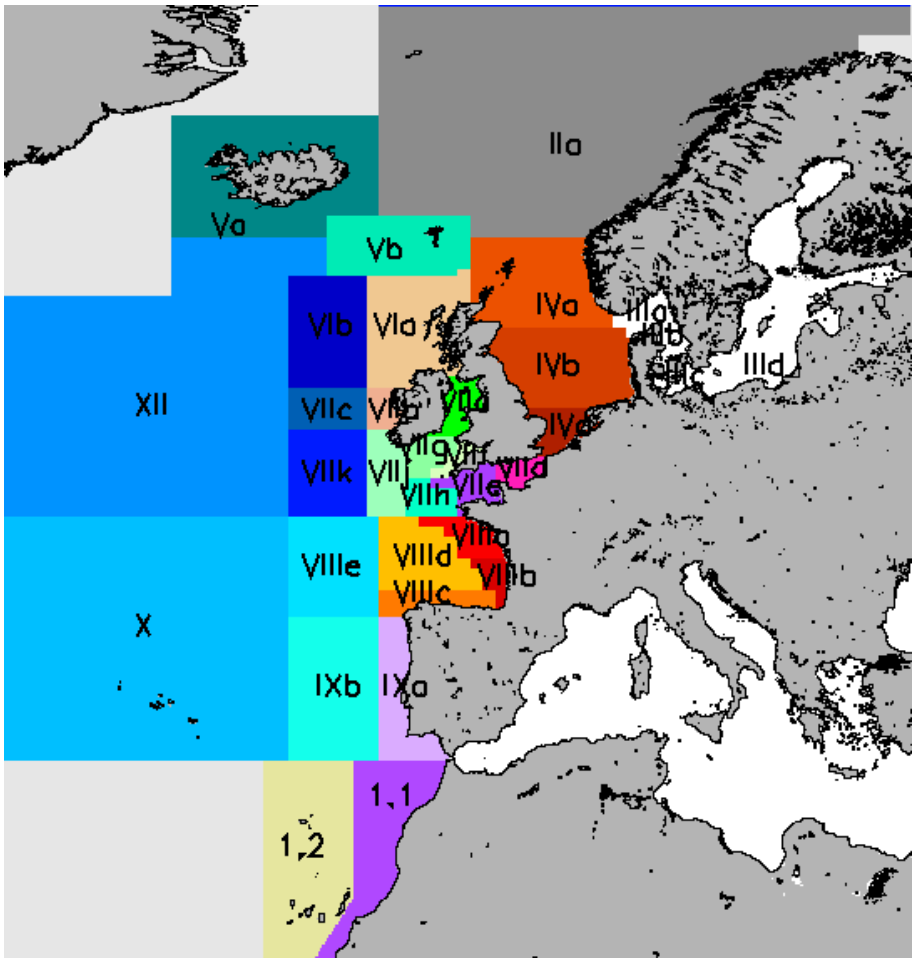

Figure 1.4: Partition of the Atlantic European waters, following ICES/FAO numbering. Acronyms (used in the text) are defined arbitrarily and do not necessarily match exact geographical limits. Groups of sub-divisions are indicated by similar colors. **NORW**: Norwegian Sea (region **IIa**); **ICES**: Iceland shelf (**Va**); **FARP**: Faroe Plateau (**Vb**); **NORS**: North Sea (regions **IVa** to **IVc**, brown); **NWBI**: northwestern British coasts (regions **VIa** and **VIIb**, cream); **IRIS**: Irish Sea (**VIIa**); **CELS**: Celtic Sea (regions **VIIf**, **g**, **h**, **j**, green); **ENGC**: English Channel (regions **VIId** and **VIIe**, purple); **NEAT**: northeast Atlantic (region **XII**); **NWSL**: northwest slope (regions **VIb**, **VIIc** and **VIIk**, blue); **BISC**: coastal Bay of Biscay (regions **VIIIa** and **VIIIb**, red); **BISO**: offshore Bay of Biscay (regions **VIIIc** and **VIIId**, orange); **IBEU**: Iberian upwelling (**IXa**); **AZORB**: Azores basin (region **X**); **SWSL**: southwest slope (regions **VIIIe** and **IXb**, light blue); **MORU**: Moroccan upwelling (**1.1**); **CANI**: Canary Islands region (**1.2**). The latter two provinces are part of FAO region 34, all the others part of region 27.

1.3 Statistical Analysis

This section describes the statistical analysis performed on the satellite monthly data records, expressed on a grid-point basis or as area averaged series.

Before the analysis of the time series, potential outliers are removed. First, a subset of data points is constructed for each month m by taking the value associated with m for all years, and the corresponding average $\overline{X}_m$ and standard deviation σ_m are computed. Data points lying beyond the range $[\overline{X}_m \pm 3\sigma_m]$ are excluded as unrealistic values (in practice considered too far from climatology). Moreover, the coverage of the satellite derived data is variable and can be almost completely missing during some months (typically during winter at high latitudes). These differences in temporal coverage are treated as follows. If valid values for the month m are present less than 50% of the years, all values for m are removed, in effect creating synthetic time series with a seasonal cycle of varying length, or period P <12. The eventual remaining missing data have been filled using the eigenvectors filtering method described in Ibanez and Conversi (2002), which presents the advantage of preserving the temporal structure imbedded in the series. In any case, the percentage of data points to be filled remained lower than 5% for the whole data set for area averaged time series. For single grid points, for which this percentage increases, only time series with less than 25% of missing values have been considered.

Monthly time series (X_t) can be considered as the sum of three components (Shiskin, 1978):

$$X_t = S_t + T_t + I_t \tag{1.1}$$

where S_t represents the seasonal term, T_t the trend and I_t the irregular or residual component (i.e., signal which is not described by the trend and the seasonal terms). Various methods have been proposed in order to individuate each of these components (Makridakis et al., 1998). A simple decomposition approach is to assume that seasonal fluctuations are stable and rigorously periodical during the period investigated, and to consider that the long term trend can be described by a linear function (e.g., Yurganov et al., 1997).

The time series decomposition procedure can be summarized by the following steps. First, X_t is smoothed by a moving average excluding all the periodical (seasonal) variations. Classically, a 13-term centered weighted moving average ($MA_{2\times12}$ is used in order to eliminate the constant seasonality of order 12 while keeping the linear trends and minimizing the variance of the irregular component, Shiskin, 1978). In the present case, the smoothing procedure needs to consider the specific annual periodicity P (in months) associated with each of the time series. Thus, the classical filter $MA_{2\times12}$ has been substituted by $MA_{2\times P}$ (P+1 terms centered weighted running mean) if P is even or by MA_P (P terms centered running mean) if P is odd, as recommended by Pezzulli et al. (2005). Moving averages induce the exclusion of some data at the extremities of the time series, and several methods have been suggested to overcome this problem (Findley et al., 1998). A simple approach consists in replicating the first and last values until necessary (i.e., "circular method", Pezzulli et al., 2005).

The smoothed series is then subtracted from the original series X_t and the resulting values are averaged for each month of the year, yielding the seasonal component of the series S_t. The deseasonalized series, (X_t - S_t), represents the sum of the trend

and irregular terms (T_t + I_t). The trend component T_t is extracted by applying a linear least square regression on (X_t - S_t). The statistical significance of the linear change in the deseasonalized series revealed by T_t (i.e., the slope of the regression) is estimated by a Student's t-test. The irregular term I_t, representing both the inter- and sub-annual variations of the time series, is finally isolated by subtracting T_t from the seasonally adjusted series (X_t - S_t).

The total variance σ_X^2 of the original time series X_t can now be written as:

$$\sigma_X^2 = \sigma_S^2 + \sigma_T^2 + \sigma_I^2 + 2\, cov(T_t, S_t, I_t) \tag{1.2}$$

where σ_S^2, σ_T^2 and σ_I^2 represent the variance associated with the seasonal, trend and irregular components respectively and $cov(S_t, I_t, T_t)$ is the covariance terms between these components. The covariance term accounts for only a small percentage of the total variance (typically <5% in absolute value), and for practical purposes, the relative contribution of each component to the total variance, defined as $\tilde{\sigma}^2$ and expressed in percent, is simply approximated by $\tilde{\sigma}^2 = 100\ \sigma^2\ /\ (\sigma_S^2+\sigma_T^2+\sigma_I^2)$.

Section 2

Temporal Variability of Optical Properties

This section describes the patterns of temporal variability for SeaWiFS L_{WN} and band ratio monthly time series in the various European regions. It specifically focuses on the analysis of both spatial and spectral variations of the relative contributions of the seasonal and non-seasonal (i.e., irregular and trend) variability. In general, the relative weight associated with the trend component remains relatively low (<15 %) certainly in relation with the assumption of linear changes. For each major domain, a specific analysis of the long term trends is then developed.

2.1 Mediterranean Sea

2.1.1 Seasonal and Irregular Variances

In the Mediterranean Sea, the L_{WN} time series at 412, 443 and 490 nm are characterized by a very high contribution of the seasonal component, with a percentage of σ_S^2 to the total variance of the monthly time series between 71% and 96% if the Adriatic Sea is excluded (Fig. 2.1). The prevalence of a stable and strong seasonal cycle for SeaWiFS water-leaving radiances at blue wavelengths underlines the importance of the variations in the marine biological activity for driving the dynamics of the optical properties in the Mediterranean ecosystems. This general result is modulated by some specific regional features, where $\tilde{\sigma}_I^2$ is relatively higher. This is true in the northern part of the Aegean Sea (AEGS), a case likely related to the outflow of local rivers and the Sea of Marmara (e.g., Karageorgis et al., 2008). Higher values of $\tilde{\sigma}_I^2$ are also observed in the coastal regions of the Gulf of Lions (GLIO), particularly west of the Rhône River outlet (dilution area, Lefèvre et al., 1997) and secondarily for L_{WN} at 412 and 443 nm in the offshore region characterized by a large space and time variability of the phytoplankton biomass (e.g., Marty et al., 2002; Nezlin et al., 2004). The fact that the spring bloom in this region is impacted by mesoscale variability (Lévy et al., 1999) also contributes to an increase in $\tilde{\sigma}_I^2$. In the Alboran Sea (ALBS), an examination of the maps of $\tilde{\sigma}_I^2$ (not shown) reveals high values associated with the location of the Alboran anticyclonic gyre where large Chl$a$ can be observed. Optical variability has been documented across the jets and fronts found in this region (Claustre et al., 2000; Ruiz et al., 2001). Besides these regional features, $\tilde{\sigma}_I^2$ for $L_{WN}(490)$ is also greater than 50% over a large part of the Mediterranean coastlines. The results are more

contrasted in the Adriatic Sea; for instance, the irregular component accounts for 69% of the variance of $L_{WN}(443)$ in the northern Adriatic Sea (NADS), and $\tilde{\sigma}_S^2$ and $\tilde{\sigma}_I^2$ are nearly equal at 490 nm for both central and southern Adriatic (Fig. 2.1). The optical properties in this basin are affected by coastal and river inputs, particularly along the Italian coasts, and circulation features associated with wind forcing and mesoscale variability (Bignami et al., 2007; Mauri et al., 2007). In addition, a variable phytoplankton bloom is a feature of the southern basin (Santoleri et al., 2003).

Globally, the contribution of the seasonal component at 555 and 670 nm is the dominant variance term of the area-averaged time series but at a lower level with respect to the blue wavelengths. Seasonal and irregular variances are found comparable in the most oligotrophic waters of the eastern Mediterranean (i.e., $\tilde{\sigma}_S^2 \leq 60\%$, in the South Ionian and Levantine provinces, Fig. 2.1), when compared to the other parts of the basin. This is likely related to the low variability for green and red wavelengths (of a very low amplitude for the latter) existing in phytoplankton-poor waters. On a grid point basis, the irregular term tends to be higher than for the area-averaged time series, particularly in oligotrophic waters, again underlining a lower signal-to-noise ratio of the L_{WN} record at these wavelengths.

The general dominance of the seasonal fluctuations breaks down for the radiance signal at 510 nm. Actually, $\tilde{\sigma}_S^2$ has a clear spectral minimum at 510 nm (and $\tilde{\sigma}_I^2$ a maximum), except for the Adriatic Sea where the variability of scattering likely impacts $L_{WN}(510)$ (Fig. 2.1). In the framework of a case-1 water bio-optical model, the reflectance spectrum around 510-520 nm does not vary strongly with Chl$a$ (Morel and Maritorena, 2001). The result obtained here is the signature of this "hinge" point (or inflection point, Clark et al., 1970) for the Mediterranean open waters.

Logically, the time series for band-ratios between 412 and 490 nm present a very high seasonality, with $\tilde{\sigma}_S^2 > 80\%$ in most cases (63% for $\rho(490)$ in the northern Adriatic Sea). This general result holds for Chl$a$ and $K_d(490)$ as well. This is shown by Fig. 2.1 and is confirmed by the related maps, with some variations due to specific features mentioned previously for L_{WN} between 412 and 490 nm. In line with the results observed at 510 nm, the seasonal component of $\rho(510)$ has a lower relative variance than the other band ratios.

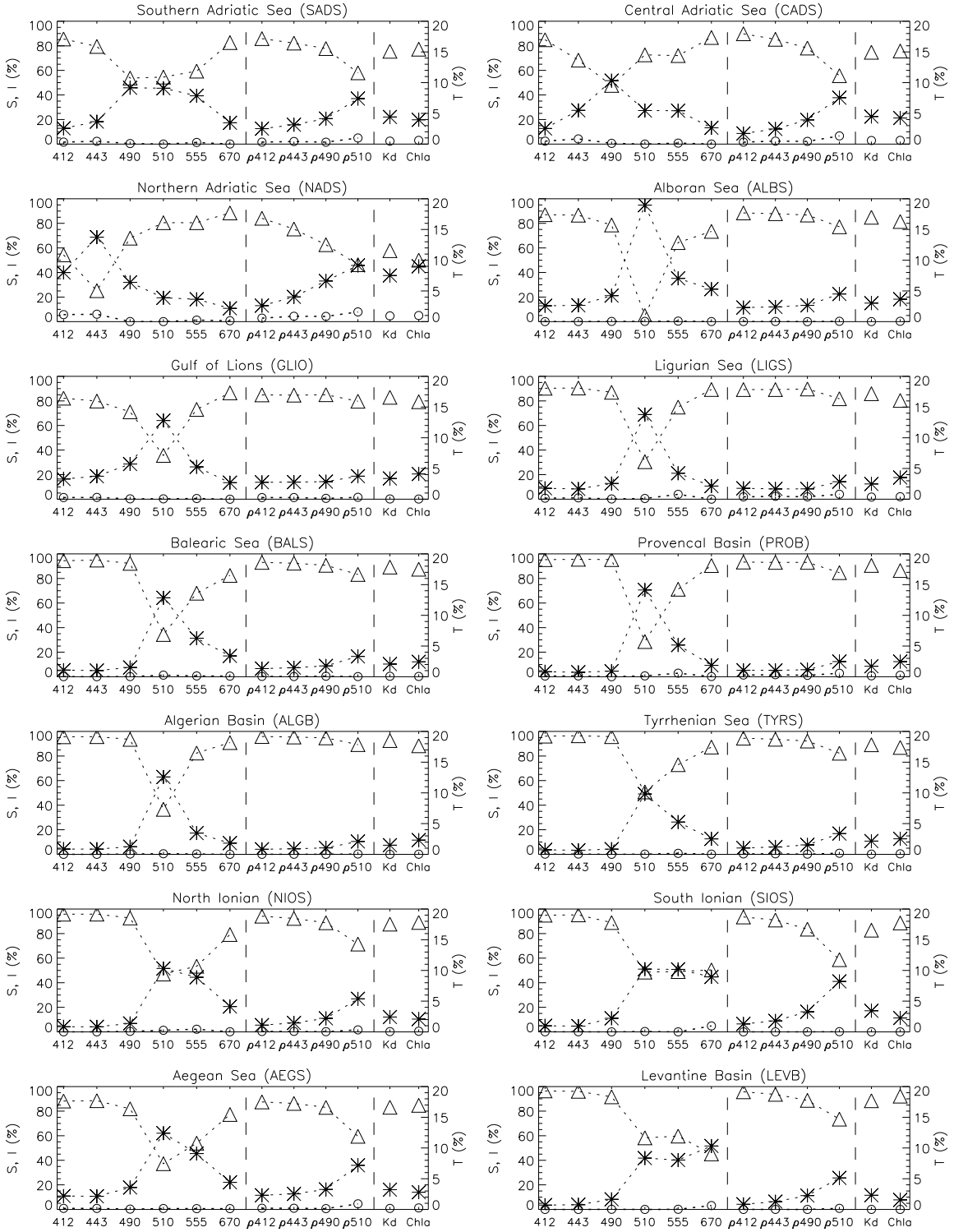

Figure 2.1: Relative contribution (in %) of the seasonal ($\tilde{\sigma}_S^2$, '$\triangle$'), irregular ($\tilde{\sigma}_I^2$, '$*$') and trend ($\tilde{\sigma}_T^2$, '$\circ$') components to the total variance of the time series for SeaWiFS radiances (at 412, 443, 490, 510 and 555 nm), band ratios (ρ_{412}, ρ_{443}, ρ_{490}, ρ_{510}), chlorophyll a (Chl$a$) and attenuation coefficient at 490 nm ($K_d(490)$) in the Mediterranean Sea.

2.1.2 Trend Analysis

The variance due to the trend does not exceed 8% for the area averaged time series, a result that remains mostly true on a grid point basis, except for some isolated points. Relevant (negative) trends, with varying levels of significance, are mainly detected for L_{WN} at 412 and 443 nm in the Algerian, Aegean and Levantine Basins (-0.56% a^{-1}, with $p< 0.001$ in the latter case, Table 2.1 and Fig. 2.2). Increases in $L_{WN}(443)$ can be observed in some parts of the Ionian Sea (Fig. 2.2). The trend for $L_{WN}(490)$ is found negative (-0.22% to -0.60% per year) for most of the basin, with $p< 0.001$ for six regions. For a lower number of areas, L_{WN} at 510 and 555 nm are also found significantly decreasing (see also Fig. 2.3). The strongest decrease can be noticed for $L_{WN}(555)$ in NADS (-1.60% a^{-1}). Overall, this decrease of L_{WN} that is detected across the spectrum could be explained by a decrease in concentrations of scattering particles.

	L_{WN}					ρ					
	412	443	490	510	555	412	443	490	510	$K_d(490)$	Chl$a$
S. Adriatic (SADS)	-	-	-0.44^{**}	-0.35^{*}	-0.64^{**}	-	-	-	0.27^{**}	-	-
C. Adriatic (CADS)	-	-	-0.44^{*}	-0.45^{*}	-0.89^{***}	0.93^{**}	0.84^{***}	0.39^{*}	0.42^{***}	-0.66^{**}	-1.42^{***}
N. Adriatic (NADS)	-	-	-	-	-1.60^{***}	2.06^{***}	2.13^{***}	1.61^{***}	1.19^{***}	-2.00^{***}	-3.44^{***}
Alboran S. (ALBS)	-	-0.41^{*}	-0.60^{***}	-0.27^{*}	-	-	-	-0.56^{**}	-	1.05^{**}	1.47^{*}
G. Lions (GLIO)	-	-	-	-	-0.45^{*}	-	-	-	-	-	-
Ligurian S. (LIGS)	-	-	-0.40^{**}	-0.30^{**}	-0.59^{***}	-	-	-	0.29^{*}	-	-
Balearic S. (BALS)	-	-0.30^{*}	-0.41^{***}	-	-	-	-	-0.39^{*}	-	0.74^{*}	-
Provencal B. (PROB)	-	-	-0.22^{*}	-	-0.33^{*}	-	-	-	0.28^{*}	-	-
Algerian B. (ALGB)	-0.53^{**}	-0.41^{**}	-0.46^{***}	-	-	-	-	-	-	0.64^{*}	-
Tyrrhenian S. (TYRS)	-	-	-0.32^{***}	-0.18^{*}	-0.43^{**}	-	-	-	0.26^{**}	-	-
N.Ionian S. (NIOS)	-	-	-0.26^{***}	-0.26^{*}	-0.61^{***}	0.57^{**}	0.59^{**}	0.34^{*}	0.36^{***}	-0.55^{*}	-1.06^{**}
S.Ionian S. (SIOS)	-	-	-	-	-	-	0.38^{*}	-	0.23^{*}	-	-
Aegean S. (AEGS)	-0.38^{*}	-0.28^{*}	-0.35^{***}	-	-	-	-	-	-	-	-
Levantine B. (LEVB)	-0.56^{***}	-0.43^{***}	-0.43^{***}	-	-	-	-	-	-	-	-

Student t-test probability : – : NS, * : p<0.05, ** : p<0.01,*** : p<0.001

Table 2.1: Percentage of long term linear changes in SeaWiFS derived radiances (at 412, 443, 490, 510 and 555 nm), band ratios (ρ_{412}, ρ_{443}, ρ_{490}, ρ_{510}), chlorophyll a (Chl$a$) and attenuation coefficient at 490 nm ($K_d(490)$) from November 1997 to October 2007 (in % a^{-1}) in the Mediterranean Sea. See Fig. 1.1 for a complete definition of the regions.

Significant trends for band ratios affected only a few regions, mostly the Adriatic and the north Ionian Seas (>0 for all band ratios), and the Alboran and Balearic Seas (<0 for $\rho(490)$). The largest and highly significant trend is found for the northern Adriatic, with approximately +2.1% a^{-1} for $\rho(412)$ and $\rho(443)$ (Table 2.1). Consequently, opposite trends are found for $K_d(490)$ and Chl$a$ in these regions (see also Fig. 2.5 and 2.6). The distributions of trends for band ratios is illustrated by the corresponding map for $\rho(443)$ which is fairly representative of trend patterns for the band ratios (Fig. 2.4).

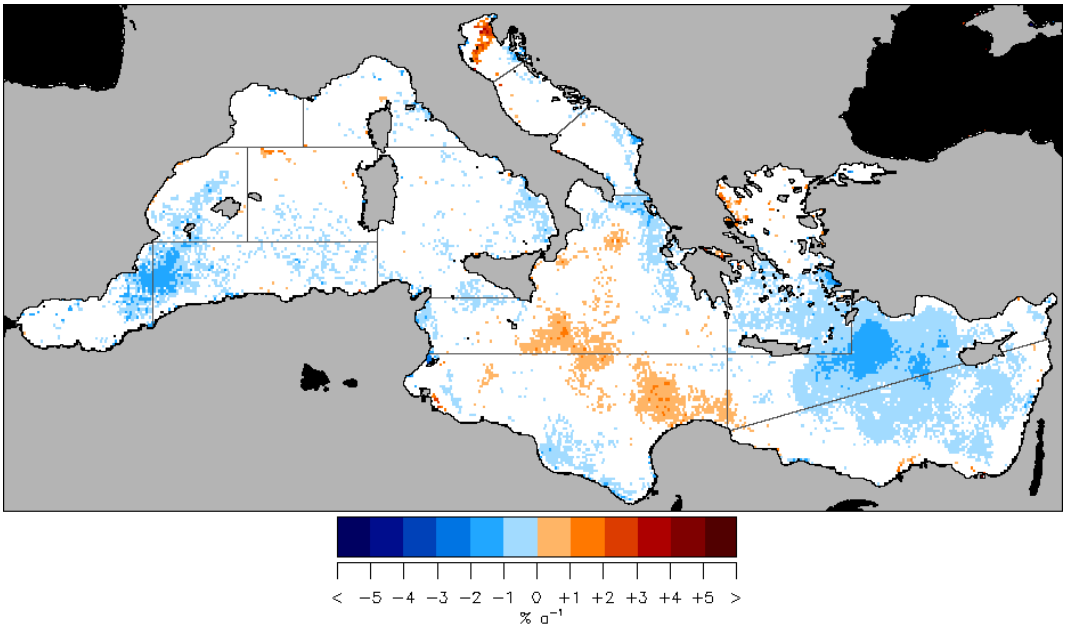

Figure 2.2: Relative linear changes in $L_{WN}(443)$ over the 10-year period SeaWiFS record (from November 1997 to October 2007, in % a^{-1}) in the Mediterranean Sea. Only the pixels for which a significant linear trend has been detected are reported ($p < 0.05$).

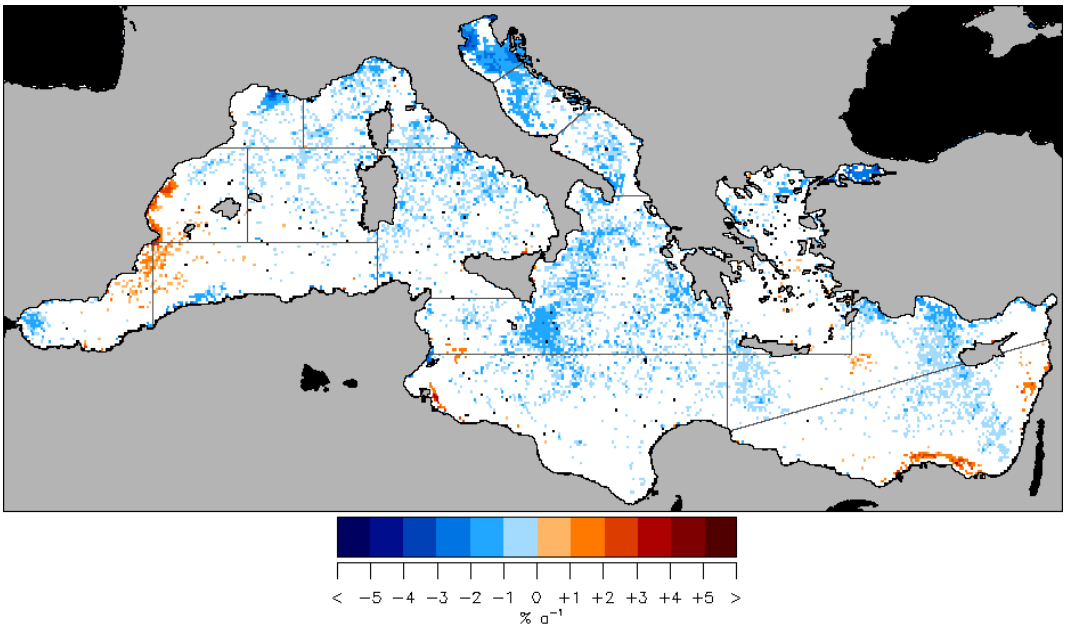

Figure 2.3: Relative linear changes in $L_{WN}(555)$ over the 10-year period SeaWiFS record (from November 1997 to October 2007, in % a^{-1}) in the Mediterranean Sea. Only the pixels for which a significant linear trend has been detected are reported ($p < 0.05$).

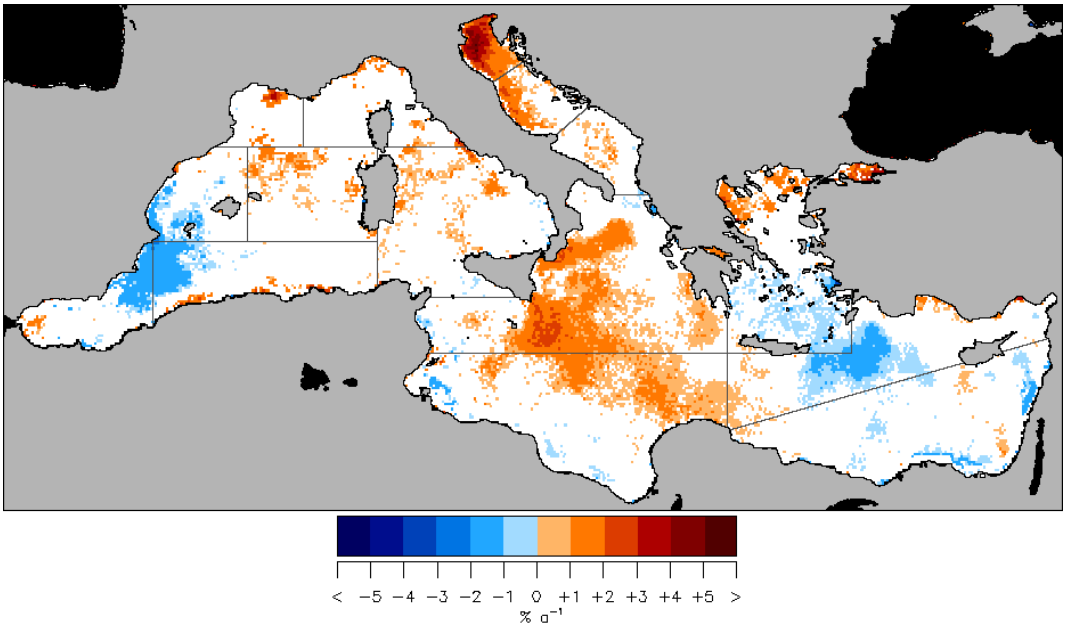

Figure 2.4: Relative linear changes in the band ratio $\rho(443)$ over the 10-year period SeaWiFS record (from November 1997 to October 2007, in % a^{-1}) in the Mediterranean Sea. Only the pixels for which a significant linear trend has been detected are reported ($p < 0.05$).

In the Adriatic, the largest trend signals are found close to the Po River outflow, along the Italian coasts, and secondarily in the location of the southern Adriatic bloom (Fig. 2.4 to 2.6). The studies of Bernardi Aubry et al. (2004) and Tedesco et al. (2007) have reported an absence of changes in phytoplankton community composition and Chl$a$, respectively, in the northern Adriatic Sea. However, the time scale of these studies is different and the measurements were conducted on discrete stations, mostly north of the Po River delta. Additionally, phytoplankton pigments are not the sole driver of optical variability in this area. Still, the trend in NADS can, at least partly, be interpreted as a decrease in Chl$a$; indeed, even though overestimated, the SeaWiFS derived Chl$a$ is well correlated with the observations in the region north of the Po River outflow (Mélin et al., 2007).

A positive signal in $\rho(443)$ is widespread in the Ionian Sea, particularly southeast of Sicily, and conversely a negative signal is found at the intersection of the Alboran, Algerian and Balearic basins (Fig. 2.4). Thus the results for trend analysis performed on a point by point basis globally confirm the features previously pointed out from the regional average time series. However, they also reveal the presence of relevant changes in water optical properties occurring at smaller scales that are totally or partially masked in regional statistics. For instance, negative trends in $\rho(443)$ (waters relatively greener) and positive trends for $K_d(490)$ and Chl$a$ (Fig. 2.5 and 2.6) can be noticed southeast of Crete. The latter feature might be related to the recurrent bloom developing in the Rhodes Gyre (e.g., D'Ortenzio et al., 2003) and to the location of the Ierapetra Eddy, a zone of large, and recently increasing, eddy kinetic energy (Pujol and Larnicol, 2005). These changes are associated with an increase in $K_d(490)$, approximately +2.5% a^{-1}. A positive trend for $\rho(443)$ affects the northern part of AEGS. Except for an independent

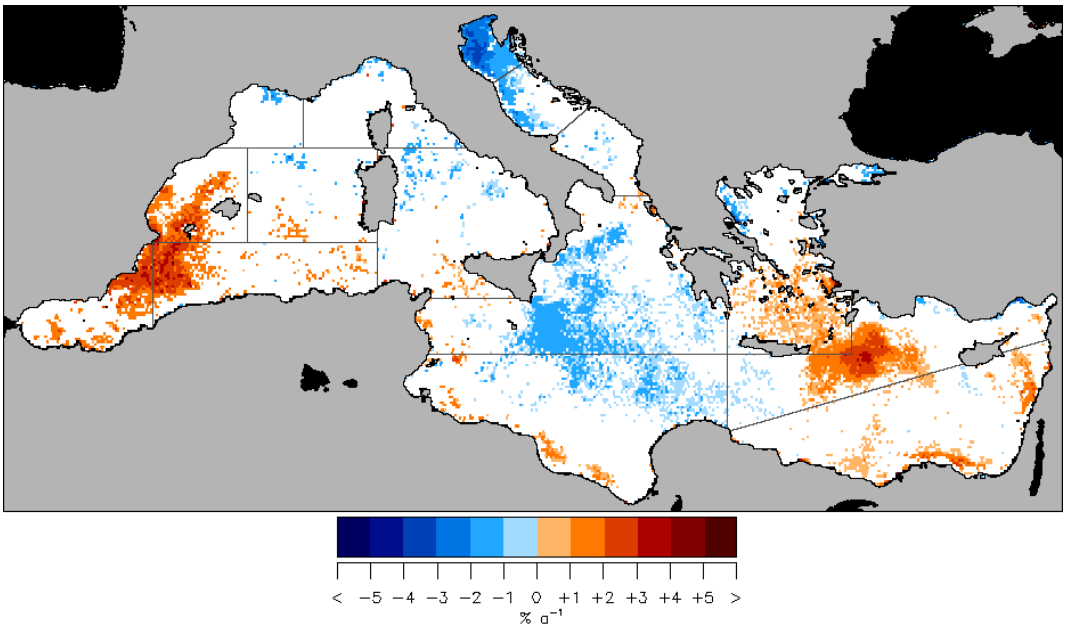

Figure 2.5: Relative linear changes in the diffuse attenuation coefficient $K_d(490)$ over the 10-year period SeaWiFS record (from November 1997 to October 2007, in % a^{-1}) in the Mediterranean Sea. Only the pixels for which a significant linear trend has been detected are reported ($p < 0.05$).

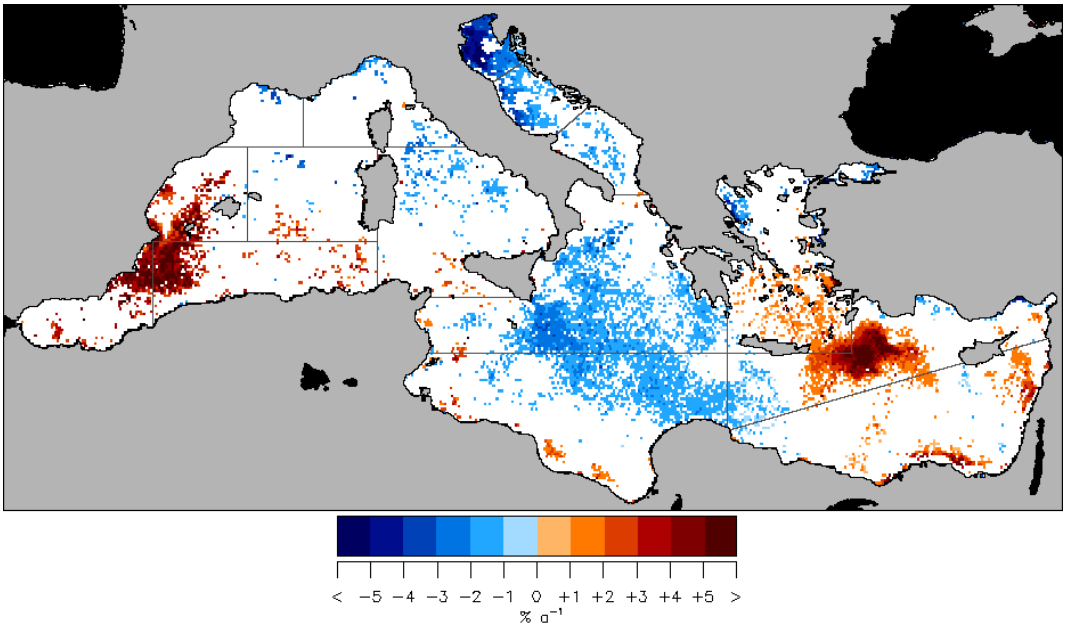

Figure 2.6: Relative linear changes in the chlorophyll a concentration Chl$a$ over the 10-year period SeaWiFS record (from November 1997 to October 2007, in % a^{-1}) in the Mediterranean Sea. Only the pixels for which a significant linear trend has been detected are reported ($p < 0.05$).

feature in the GLIO associated with the Rhône River outflow, no significant trend is noticed in the northwest Mediterranean. Negative and positive trends in Chl$a$ have been documented, respectively by Goffart et al. (2002) for the Bay of Calvi (Corsica) and by Marty et al. (2002) at an offshore station in the Ligurian Sea, but both studies use data up to 1999.

2.2 Black Sea

2.2.1 Seasonal and Irregular Variances

In general, the relative contribution of the seasonal component to the total variance of the time series in the Black Sea is relatively low, ranging between 8 and 69% for all variables (Fig. 2.7). Clearly, for all the SeaWiFS bands, the percentage of variance related to the seasonal cycle, $\tilde{\sigma}_S^2$, follows an increasing gradient from the more turbid water masses of the western shelf (32-46%) and Sea of Marmara (31-54%) to clearer waters in the eastern part of the basin (55-69%, Fig. 2.7). This is associated with a reciprocal decreasing gradient of the relative contribution of σ_I^2, varying from 29-34% in the eastern part (43% at 670 nm) up to 66% for the western shelf region. These results are consistent with the observations of Oguz et al. (2002) who underlined the links between meso- and sub-mesoscale structures (like filaments, meanders) and the ocean color signal in the northwestern Black Sea, and with the work of Kopelevich et al. (2002) who noticed that the seasonal Chl$a$ signal (derived from Coastal Zone Color Scanner data) was more pronounced in the deep Black Sea than on the shelf. Strong optical signatures at basin scale are also due to large blooms of coccolithophores, that contribute to both seasonal and irregular components of L_{WN} considering their occurrence around June but with varying extent, duration and intensity (Cokacar et al., 2004; Karabashev et al., 2006). The spatial heterogeneity in the temporal dynamics of the Black Sea optical properties underline the diversity of environmental parameters driving the dynamics of the optically significant components of seawater.

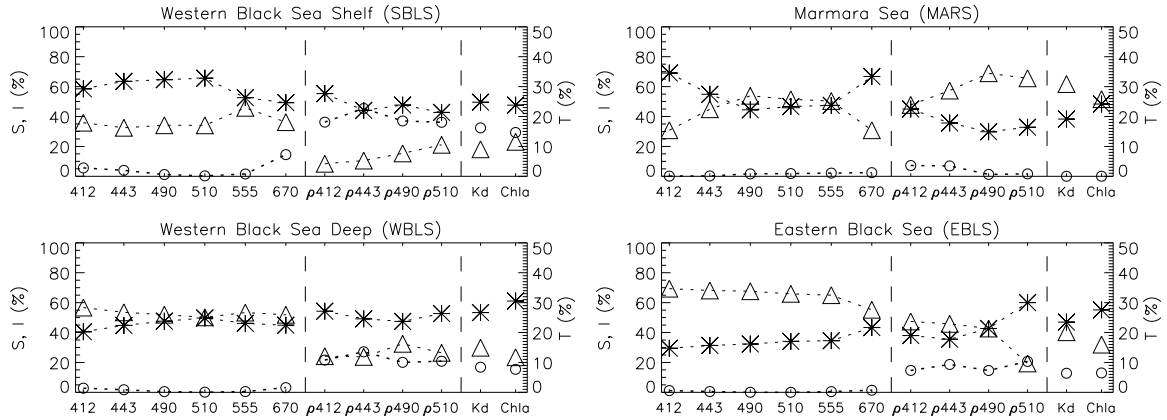

Figure 2.7: Relative contribution (in %) of the seasonal ($\tilde{\sigma}_S^2$, '△'), irregular ($\tilde{\sigma}_I^2$, '∗') and trend ($\tilde{\sigma}_T^2$, '○') components to the total variance of the time series for SeaWiFS radiances (at 412, 443, 490, 510 and 555 nm), band ratios (ρ_{412}, ρ_{443}, ρ_{490}, ρ_{510}), chlorophyll a (Chl$a$) and attenuation coefficient at 490 nm ($K_d(490)$) in the Black Sea.

A west-east gradient of increasing variance contribution of the seasonal cycle is also seen for the band ratios (except for $\rho(510)$) as well as for $K_d(490)$, but $\tilde{\sigma}^2_S$ is lower than for L_{WN}. Interestingly this is accompanied by a gradient of decreasing contribution due to trend $\tilde{\sigma}^2_T$ for the band ratios, from 36-45% on the western shelf to 15-21% in the eastern basin (Fig. 2.7), and similarly, $\tilde{\sigma}^2_T$ decreases from 32% to 13% for $K_d(490)$.

2.2.2 Trend Analysis

The contribution of the trend to the total variance corresponds to highly significant trends that are detected for all SeaWiFS band ratios (positive trends), as well as $K_d(490)$ and Chl$a$ (negative trends), in the three regions considered for the Black Sea (Table 2.2, p<0.01 for $\rho(412)$, p<0.001 otherwise). Importantly, results relying on regional average time series are fully in line with those obtained on a spatial basis (see Fig. 2.9 and 2.10). On the other hand, for L_{WN}, significant trends (p<0.05) are found only between 412 and 490 nm in the deep basin (approximately +2% a^{-1}), and these changes are mostly affecting the northern parts (Fig. 2.8). Upward changes in band ratios tend to be stronger for time series related to the shortest SeaWiFS wavelengths, $\rho(412)$ and $\rho(443)$ (Table 2.2). For instance in the deep west Black Sea region, an increase of +2.1% a^{-1} for these ratios is noted while it is of +1.0% a^{-1} for $\rho(510)$. Moreover, changes in optical quality of the water masses are slightly more pronounced in the western Black Sea than in the eastern part of the basin (e.g., +2.1% versus 1.9% per year for $\rho(412)$ and $\rho(443)$, Table 2.2, see also Fig. 2.9). Interestingly the trends for band ratios, $K_d(490)$ and Chl$a$ over the western shelf are essentially found in the southern part (Fig. 2.9 and 2.10). The significant increase observed for $\rho(490)$ is obviously translated into a large decrease of $K_d(490)$ values. Over the 10-year period, regional statistics indicate that $K_d(490)$ decreased by approximately -1.7% a^{-1} over the basin (Table 2.2). Finally, the standard Chl$a$ product indicates a trend of approximately -3% a^{-1}. Positive trends for ρ are also observed in the Sea of Marmara, associated with negative trends for L_{WN} at 510 and 555 nm.

	L_{WN}					ρ					
	412	443	490	510	555	412	443	490	510	$K_d(490)$	Chl$a$
Black S. Shelf (SBLS)	-	-	-	-	-	1.44**	1.65***	1.34***	1.06***	−1.60***	−3.03***
W.Black S. Deep (WBLS)	2.28*	2.40*	1.89*	-	-	2.10**	2.14***	1.58***	1.02***	−1.82***	−3.09***
E.Black S. (EBLS)	2.26*	2.36**	1.97*	-	-	1.93**	1.90***	1.44***	0.96***	−1.63***	−2.73***
Marmara S.(MARS)	-	-	-	−1.83*	−2.48*	2.55**	1.89***	0.86**	0.67**	-	-

Student t-test probability : − : NS, * : p<0.05, ** : p<0.01,*** : p<0.001

Table 2.2: Percentage of long term linear changes in SeaWiFS derived radiances (at 412, 443, 490, 510 and 555 nm), band ratios (ρ_{412}, ρ_{443}, ρ_{490}, ρ_{510}), chlorophyll a (Chl$a$) and attenuation coefficient at 490 nm ($K_d(490)$) from November 1997 to October 2007 (in % a^{-1}) in the Black Sea. See Fig. 1.2 for a complete definition of the regions.

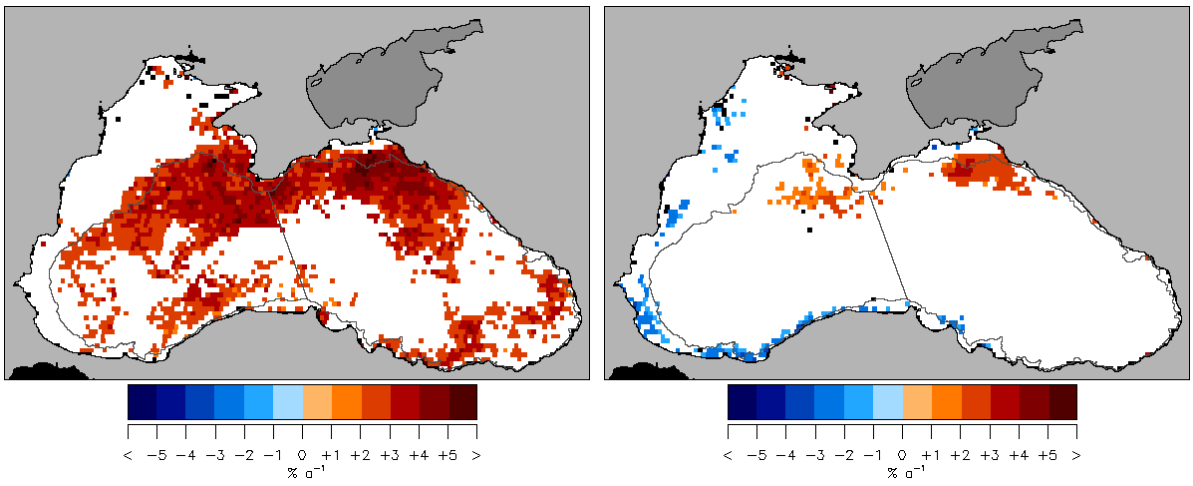

Figure 2.8: Relative linear changes in $L_{WN}(443)$ and $L_{WN}(555)$ over the 10-year SeaWiFS record (from November 1997 to October 2007, in % a^{-1}) in the Black Sea. Only the pixels for which a significant linear trend has been detected are reported ($p< 0.05$).

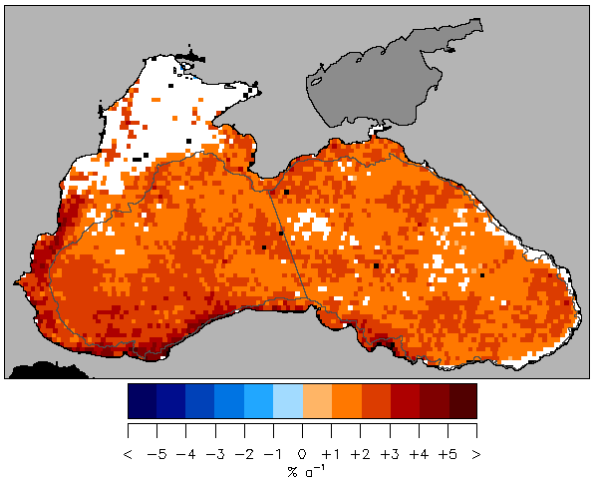

Figure 2.9: Relative linear changes in the band ratio $\rho(443)$ over the 10-year SeaWiFS record (from November 1997 to October 2007, in % a^{-1}) in the Black Sea. Only the pixels for which a significant linear trend has been detected are reported ($p< 0.05$).

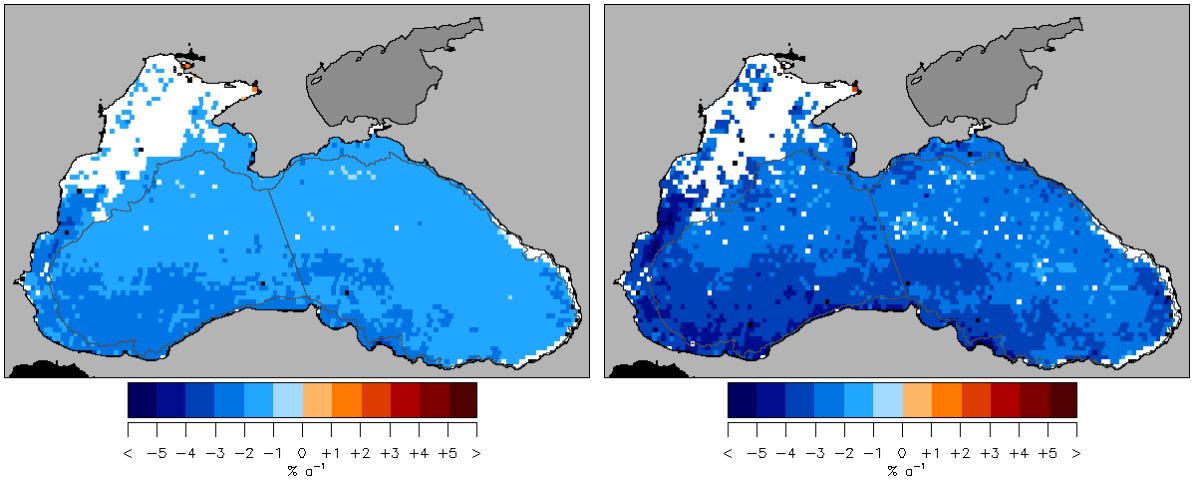

Figure 2.10: Relative linear changes in the diffuse attenuation coefficient $K_d(490)$ and chlorophyll a concentration Chl$a$ over the 10-year SeaWiFS record (from November 1997 to October 2007, in % a^{-1}) in the Black Sea. Only the pixels for which a significant linear trend has been detected are reported ($p< 0.05$).

The relative importance of the trend signal for the Black Sea is completely in line with past and current data sets documenting the interannual variability that has affected the basin. Large variations of the ecosystem components of the Black Sea in the last four decades have now been reported in terms of physics (Ginzburg et al., 2004), chemistry (Konovalov and Murray, 2001) or ecology (Kideys, 2002). They have been prompted by a complex set of pressures, including impacts from large scale climatic variability (Oguz et al., 2006), variations in the nutrient and pollutant inputs from the coast and rivers and their distribution in the basin (Humborg et al., 1997; Yunev et al., 2005), overfishing (Daskalov, 2002), and the appearance and evolution of invasive species, particularly gelatinous zooplankton (Kideys and Romanova, 2001; Kideys et al., 2005). The present study synthesizes the optical signature of these changes using the ocean color record, and work is in progress to clearly identify the associated drivers (e.g., Oguz and Gilbert 2007).

2.3 Baltic Sea

2.3.1 Seasonal and Irregular Variances

The main characteristic of time series for SeaWiFS L_{WN} and band ratios in the Baltic Sea is the overall high level of variance explained by the irregular component with respect to the other European basins. This feature is particularly pronounced for radiances at 412 and 443 nm where $\tilde{\sigma}_I^2$ is found to explain from 53% to 93% of the total variance in the vast majority of the Baltic regions (Fig. 2.11). This dominance is also found homogeneous in space. The residual term $\tilde{\sigma}_I^2$ remains the major contributor to the total variance at 490, 510 and 555 nm in the Skagerrak (SKAG), Kattegat (KATT), and the Belt (BELS) and Arkona (ARKS) Seas, and at all channels in the Northern Baltic Proper region (NBAP). Conversely, in the Gulfs of Gdansk (GGDA), Riga (GRIG) and Finland (GFIN), the Archipelago region (ARCH), the Aland Sea (ALAS), the Gotland Basin (GOTB) and the Southern Baltic Proper (SBAP), the relative contribution of the irregular component is superseded by the seasonal term as the wavelength increases, particularly at 555 nm, and to a lesser extent in the red part of the spectrum (Fig. 2.11). A singular situation is observed in the Kattegat, where a significant seasonal component is detected at 412, 443 and 670 nm, and in the Skagerrak at 412 and 670 nm, whereas the irregular term dominates between 490 and 555 nm. Similarly, the Bothnian Sea (BOTS) and Bothnian Bay (BOTB) clearly differ from the other parts of the basin since a relevant seasonal signal prevails for all the SeaWiFS radiance time series ($\tilde{\sigma}_S^2 > 50\%$ except at 555 nm in BOTB, Fig. 2.11). This might be the signature of the seasonal cycle of DOM inputs from land (Zweifel et al., 1995; Schwarz, 2005) impacting the apparent optical properties.

A wide spectral and spatial variability is also observed for the variance terms determined for radiance band ratios (Fig. 2.11). The seasonal component represents the main contributor to the total variance ($\tilde{\sigma}_S^2$ between 48% and 78%) in the Gotland Basin, the Southern Baltic Proper and to a lesser extent in the Bothnian Bay region and the Gulf of Finland (except for $\rho(412)$). Actually for the main regions of the basin (SBAP, GOTB, NBAP, GFIN) as well as for GGDA and ARKS, the seasonal contribution to the variance of ρ increases with wavelength. Inversely, the irregular variations tend to explain the major part of the temporal variability of band ratio time series in the KATT, BELS, ALAS, and ARCH areas ($\tilde{\sigma}_I^2 \approx$ 50-75%). In GRIG, SKAG and BOTS, $\tilde{\sigma}_S^2$ decreases with wavelength, being dominant only for $\rho(412)$ and $\rho(443)$. For $K_d(490)$ and Chl$a$, the terms $\tilde{\sigma}_S^2$ and $\tilde{\sigma}_I^2$ are usually and logically consistent with $\rho(490)$ and $\rho(510)$, respectively. In the case of Chl$a$, this is explained by the fact that the maximum band ratio algorithm OC4v4 tends to select $\rho(510)$ in presence of absorbing waters.

With respect to other basins, there are various factors contributing to lower seasonal contributions to the variance. First of all, because of the ocean color data coverage, the number of months used for the analysis is restricted to 9 months for most Baltic regions (down to 7 for BOTB). A higher level of cloud cover is likely to weaken the potential to accurately represent a seasonal cycle with the appropriate space and time sampling (Rantajärvi et al., 1998). Then, various studies in the Baltic illustrate that the amplitudes of L_{WN} are often low, particularly in the blue domain, with a spectral maximum shifted toward the green (Darecki et al., 2003; Siegel et al. , 2005). This specificity is related to the well known highly absorbing character of Baltic waters with a strong contribution of CDOM (e.g., Ferrari et al. 1996). Consequently, the corresponding low levels of the satellite derived L_{WN} in the Baltic Sea are more affected by noise, again

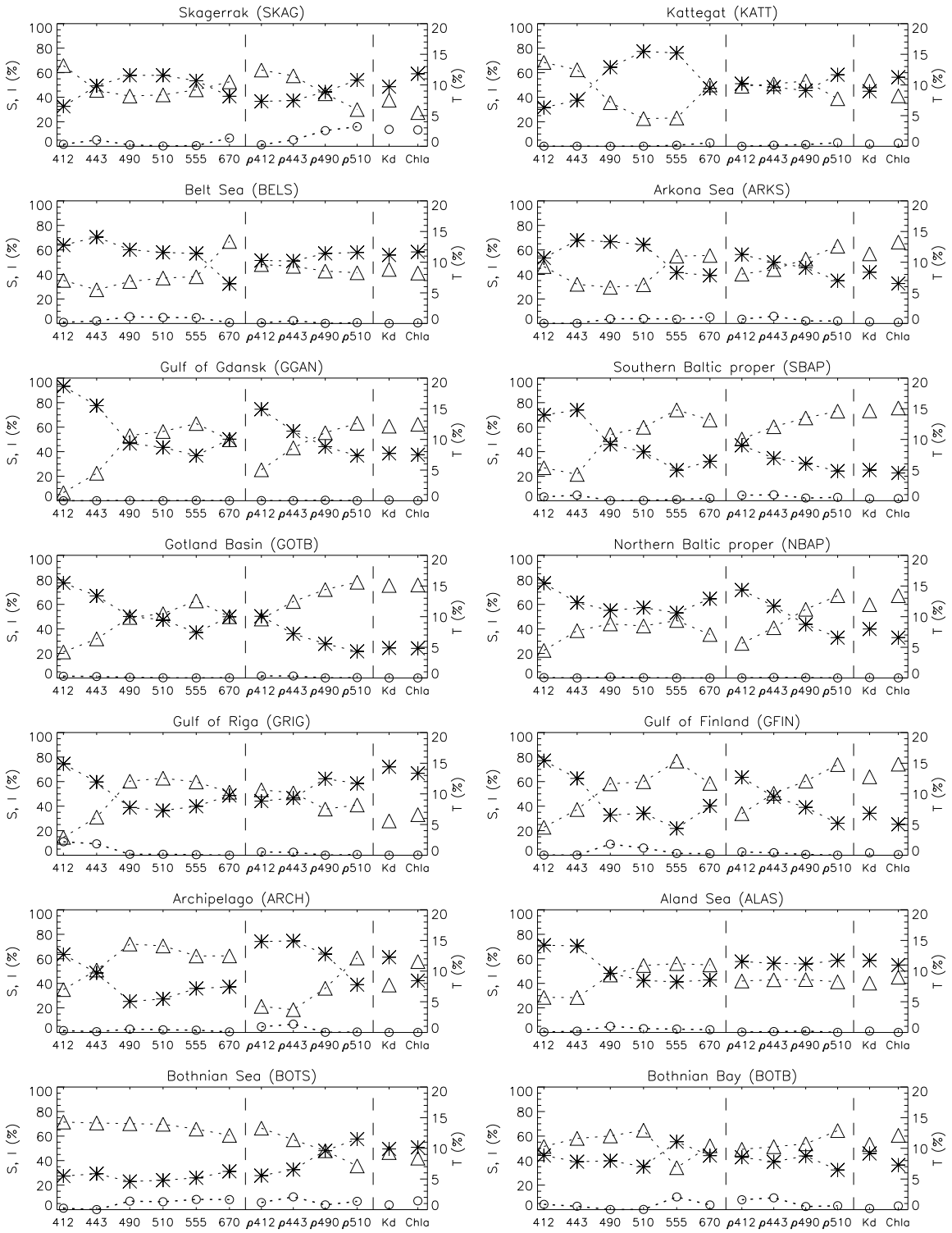

Figure 2.11: Relative contribution (in %) of the seasonal ($\tilde{\sigma}_S^2$, '△'), irregular ($\tilde{\sigma}_I^2$, '∗') and trend ($\tilde{\sigma}_T^2$, '○') components to the total variance of the time series for SeaWiFS radiances (at 412, 443, 490, 510 and 555 nm), band ratios (ρ_{412}, ρ_{443}, ρ_{490}, ρ_{510}), chlorophyll a (Chl$a$) and attenuation coefficient at 490 nm ($K_d(490)$) in the Baltic Sea.

lessening the potential to detect the seasonal signature. In the more coastal and eutrophic regions directly influenced by rivers (SBAP, GGDA, GRIG, Wasmund et al. 2001), the presence of particles counteract the absorption, and all the more efficiently in green bands. These elements do not mean that the irregular component is entirely an artifact; for instance the phytoplankton spring bloom is associated with a large degree of interannual variability (e.g., Wasmund et al. 1998; Fleming and Kaitala 2006). Another element potentially contributing to the irregular signal is the occurrence of cyanobacteria blooms with variable intensity, duration and extent. These blooms, associated with a very strong optical signature when biogenic aggregates are close to the surface, are also characterized by a high spatial variability at various scales (Kutser, 2004; Zibordi et al., 2006a) and a large interannual variability (Janssen et al., 2004; Kahru et al., 2007). On the other hand, these blooms are not necessarily well represented in the L_{WN} standard satellite records since conditions of surface accumulations are often excluded by the processing software, mostly because of typically very high L_{WN} values in the near infrared (Kutser, 2004). Finally a measure of caution is warranted for some shallow waters, particularly in the southwest corner of the Baltic Sea, where the bottom reflectance might at times impact the satellite signal (Ohde and Siegel, 2001).

2.3.2 Trend Analysis

In the Baltic Sea, long term changes in water optical properties are very heterogeneous at both spatial and spectral scales, and only few provinces show significant linear trends (Table 2.3). This overall feature might be partially related to the high levels of irregular variations observed for this basin, again emphasizing the high complexity of these waters from an optical point of view. A negative signal for $L_{WN}(490)$ can be detected for the regions KATT, BELS, and ARKS. The use of GAC data for these small coastal areas is not recommended but a significant negative trend in BELS ($p<0.05$) can also be seen over seven years with LAC data. For KATT and BELS, a corresponding decrease of $\rho(490)$ is observed (-0.5% a^{-1}, $p<0.05$), and an increase for $K_d(490)$. This is somewhat in contrast with the decreasing trends in Chl$a$ found by Wasmund and Uhlig (2003) in the Mecklenburg Bight for the period 1979-2000. Older time series indicated an increase in total suspended matter in Danish coastal waters (Højerslev, 1989). Rydberg et al. (2006) report higher values of primary production after 1997 in KATT and BELS but these are likely due to a change in measurement method; this followed a clear increase in primary production before 1980, followed by a slight negative trend in association with a reduction in nutrient loads. Consistent with this, Carstensen et al. (2004) did not detect trends in the bloom frequency using field data in the Kattegat for the period 1989-1999.

The strongest trend signals are found for the northernmost regions (Table 2.3; see also Fig. 2.15 and 2.16 in the next section). There are significant decreasing trends in ARCH, ALAS and BOTS from 490 to 555 nm, and in NBAP and GFIN at 490 and 510 nm. Consistent results could already be obtained using seven years of LAC data. A positive trend for $L_{WN}(412)$ can be observed for ARCH and BOTS. Consequently, large trends in ρ are noticeable for these regions. The increase in BOTS is +3.4% and +2.1% per year for $\rho(412)$ and $\rho(443)$, respectively. Trends in these regions might be associated with variability in inputs from land but also in physical conditions, including sea surface temperature, with a marked increase observed in this region (Siegel et al. , 2006), and sea ice (Jevrejeva et al., 2004; Meier et al., 2004). A weak positive trend can

	L_{WN}					ρ					
	412	443	490	510	555	412	443	490	510	$K_d(490)$	Chl$a$
Skagerrak (SKAG)	-	-	-	-	-	-	-	-	0.49*	-	−1.83*
Kattegat (KATT)	-	−0.90*	−1.02*	-	-	-	-	−0.56*	-	1.21**	-
Belt S. (BELS)	-	-	−1.14*	-	-	-	-	−0.53*	-	1.08**	1.69*
Arkona S. (ARKS)	-	-	−0.64*	-	-	-	-	-	-	-	-
N. Baltic (NBAP)	-	-	−1.24**	−0.95*	-	-	-	-	-	-	-
G. Finland (GFIN)	-	-	−1.09***	−0.80**	-	-	-	-	-	0.84*	-
Archipel. (ARCH)	1.94*	-	−1.11***	−1.10**	−1.20**	4.57**	2.41***	-	-	-	-
Aland S. (ALAS)	-	-	−1.71***	−1.51**	−1.68**	-	-	-	-	-	-
Bothnian S. (BOTS)	1.63**	-	−1.22***	−1.18***	−1.68***	3.38***	2.13***	0.51*	0.60***	-	−1.69**

Student t-test probability : − : NS, * : p<0.05, ** : p<0.01,*** : p<0.001

Table 2.3: Percentage of long term linear changes in SeaWiFS derived radiances (at 412, 443, 490, 510 and 555 nm), band ratios (ρ_{412}, ρ_{443}, ρ_{490}, ρ_{510}), chlorophyll a (Chl$a$) and attenuation coefficient at 490 nm ($K_d(490)$) from November 1997 to October 2007 (in % a^{-1}) in the Baltic Sea. No trend has been detected for the provinces of the Bothnian Bay (BOTB), Southern Baltic (SBAP), Gotland basin (GOTB), Gulf of Riga (GRIG) and Gulf of Gdansk (GGAN). See Fig. 1.3 for a complete definition of the regions.

be seen for $K_d(490)$ in the Gulf of Finland, where Suikkanen et al. (2007) have found an increase in summer Chl$a$ over the period 1979-2003. On the other hand, Raateoja et al. (2005) do not report trends after 1990 for the spring period at coastal stations of the Gulf. Noteworthy is the absence of trends for most variables in the Baltic Proper (ARKS, SBAP, GOTB, NBAP, Table 2.3, see also Fig. 2.14 to 2.18). Long time series have underlined trends in Chl$a$ or primary production in some of these regions (e.g., Wasmund et al., 2001; Wasmund and Uhlig, 2003; Fleming et al., 2008), and these were accompanied by changes in nutrient concentrations (Trzosińska, 1990) and Secchi depth (Sandén and Håkansson, 1996). Importantly, some of the past changes in the ecological variables of the Baltic Sea have been associated with shifts (like in the late 1980's, Alheit et al. 2005). In any case the detection of trends in terms of optically relevant quantities for the last decade and the future will require a continuous monitoring with field and satellite data. Upcoming changes might be prompted by marine protection policies, with the reduction of nutrient inputs (HELCOM, 2007a), and by multiple pressures from climate forcing including impacts on sea surface temperature and ice (HELCOM, 2007b; Siegel et al. , 2006; Meier et al., 2004). Finally, influences from invasive newcomers could also affect the Baltic ecosystem (e.g., Haslob et al. 2007).

2.4 Northeast Atlantic Domain

2.4.1 Seasonal and Irregular Variances

The distribution of the variance terms logically reflects the heterogeneity of the provinces grouped in this vast domain, including oceanic, shelf and coastal areas.

In the offshore oceanic waters, two main patterns of temporal variability can be distinguished (Fig. 2.12). First, in the southern offshore regions of the domain, the North Atlantic areas X (AZOB), VIIIe and IXb (SWSL) and the offshore waters of the Bay of Biscay (BISO, VIIIc,d) a high seasonality is detected for radiances at all wavelengths except at 510 nm, as already noted for a large part of the Mediterranean Sea. The percentage of variance represented by $\tilde{\sigma}_S^2$ for the area averaged L_{WN} series (510 nm excluded) is usually above 80% (74% for L_{WN} at 412 and 555 nm in BISO). In the Canary Islands region (CANI), large values of $\tilde{\sigma}_S^2$ (>92%) are also found for the spectral domain 412-490 nm, but $\tilde{\sigma}_S^2$ is lower for longer wavelengths (48-66%), a behavior noticed for Ionian and Levantine oligotrophic waters. Both upwelling regions (Iberian, IBEU, and Moroccan, MORU) present intermediate spectra, with $\tilde{\sigma}_S^2$ in the range 74%-89% from 412 to 490 nm, a minimum of $\tilde{\sigma}_S^2$ at 510 nm and higher values at 555 and 670 nm. Overall this dominance of the seasonal component is preserved on the corresponding maps. However, for single grid points, $\tilde{\sigma}_I^2$ tends to be the largest term for the wavelengths 510 nm and above. Moreover, $\tilde{\sigma}_I^2$ becomes dominant for the coastal strip of the upwelling provinces IBEU and MORU, regions with small-scale variability (Smyth et al., 2001; Gabric et al., 1993).

For the more northern offshore sector, the Northeast Atlantic area XII (NEAT), the areas VIb and VIIc,k (NWSL), the Faroe Plateau (FARP), and the Norwegian Sea, NORW), the largest seasonal component is detected at 555 nm ($\tilde{\sigma}_S^2$ ≈80-90% of the total variance, Fig. 2.13). Even if not as marked, the pattern is similar for the Iceland Shelf (ICES). Meanwhile, the contribution of the seasonal term is globally lower than in the southern part of the domain for radiance time series between 412 and 510 nm (from 55% to 76%) as well as at 670 nm (42-60%, except 70% for ICES). On a grid-point basis, $\tilde{\sigma}_I^2$ instead of $\tilde{\sigma}_S^2$ tends to be the dominant term, underlining how spatial averaging favors the seasonal contribution in these regions. Actually, for L_{WN} between 412 and 490 nm as well as for the corresponding ρ, $\tilde{\sigma}_S^2$ decreases sharply north of 40°N, a zone associated with a strong Chl$a$ gradient separating the North Atlantic Drift region from subtropical waters (Longhurst, 1998). Factors lowering $\tilde{\sigma}_S^2$ in the more northern waters include the local modulation of the seasonal cycle by mesoscale variability (e.g., Robinson et al., 1993; Garçon et al., 2001), interannual variations forced by the North Atlantic climate, and the effect of cloud cover on the representation of the seasonal cycle by satellite remote sensing.

For the regions described above, band ratio time series are in general highly seasonal, especially in the more oceanic regions, with $\tilde{\sigma}_S^2$ in the interval 73%-96% (69% in BISO for $\rho(412)$, and in IBEU for $\rho(510)$, Fig. 2.13). Logically, seasonality is the dominant signal for $K_d(490)$ and Chl$a$, with $\tilde{\sigma}_S^2$ in the interval 74%-91% and 68%-87%, respectively, with the exception of FARP (66% and 54%, respectively), that might be linked with large inter-annual fluctuations reported for this area (Hansen et al., 2005).

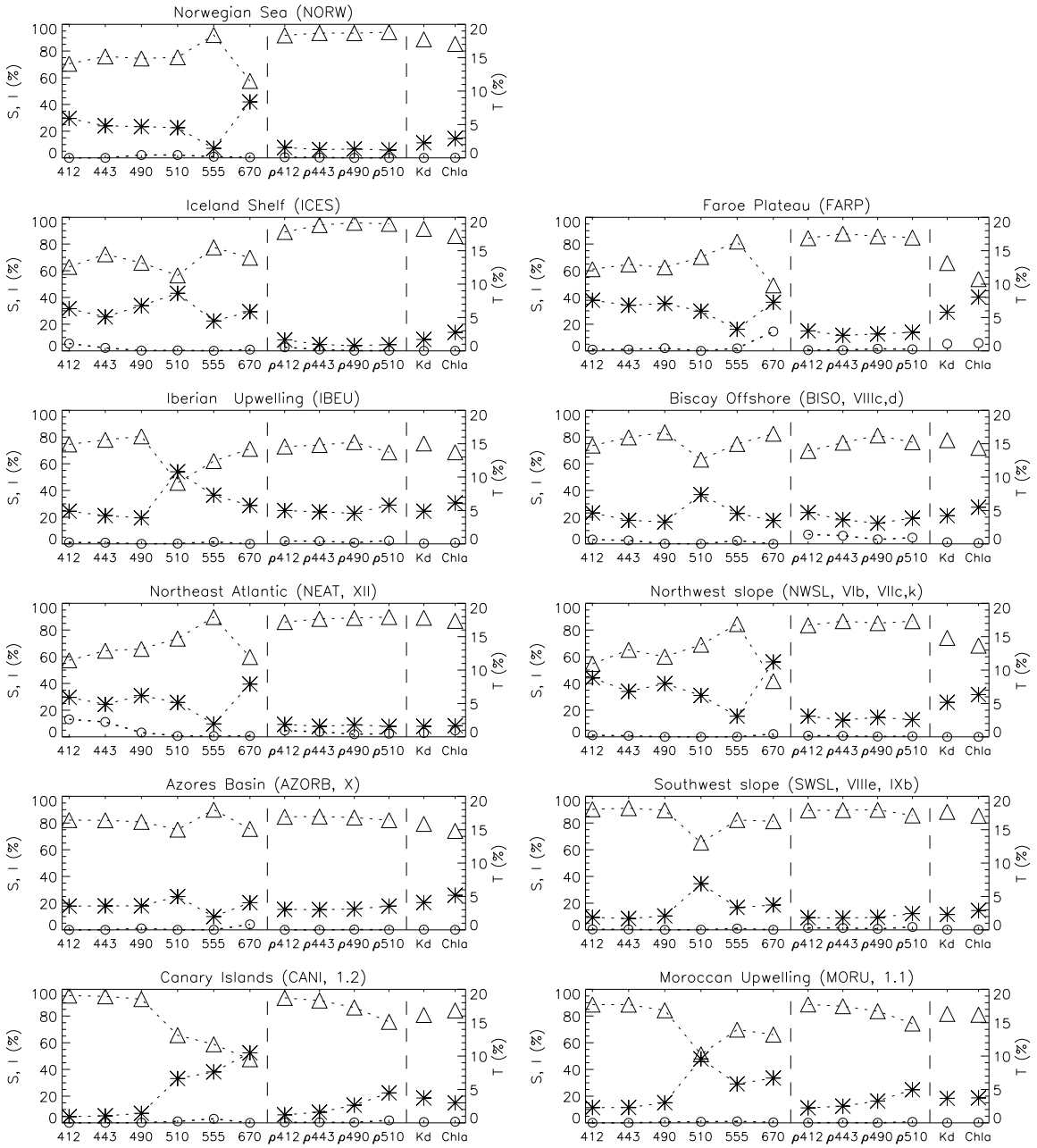

Figure 2.12: Relative contribution (in %) of the seasonal ($\tilde{\sigma}_S^2$, '$\triangle$'), irregular ($\tilde{\sigma}_I^2$, '$*$') and trend ($\tilde{\sigma}_T^2$, '$\circ$') components to the total variance of the time series for SeaWiFS radiances (at 412, 443, 490, 510 and 555 nm), band ratios (ρ_{412}, ρ_{443}, ρ_{490}, ρ_{510}), chlorophyll a (Chl$a$) and attenuation coefficient at 490 nm ($K_d(490)$) in the offshore waters of the North-East Atlantic domain. Roman numerals are for the ICES region (FAO region 27) and arabic numerals for the ICES FAO region 34.

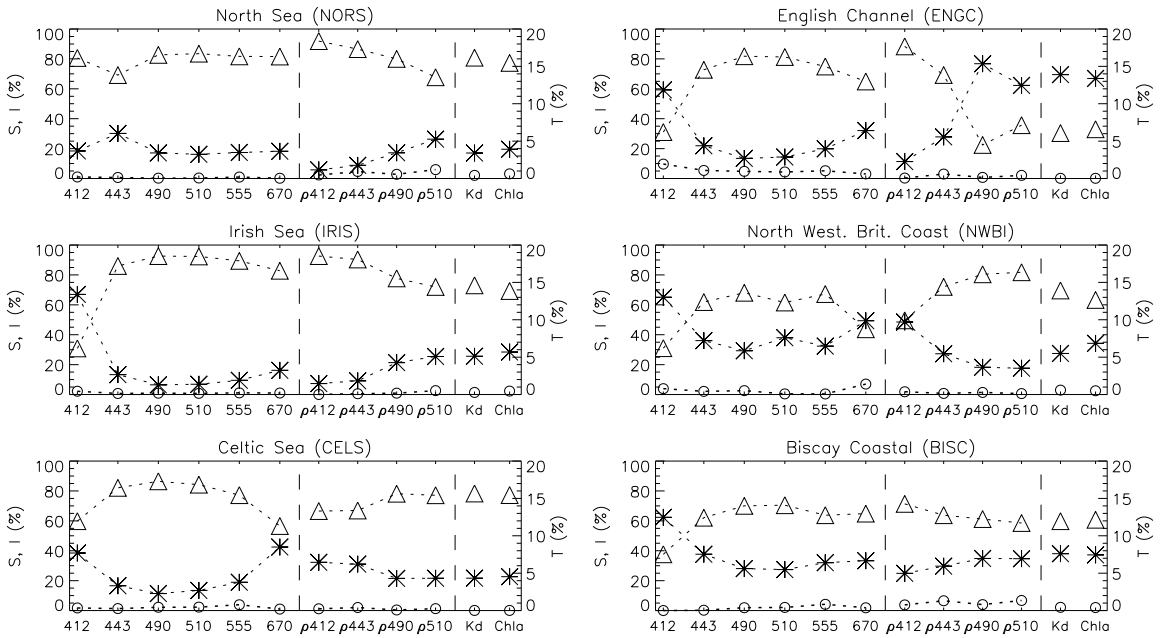

Figure 2.13: Relative contribution (in %) of the seasonal ($\tilde{\sigma}_S^2$, '△'), irregular ($\tilde{\sigma}_I^2$, '∗') and trend ($\tilde{\sigma}_T^2$, '∘') components to the total variance of the time series for SeaWiFS radiances (at 412, 443, 490, 510 and 555 nm), band ratios (ρ_{412}, ρ_{443}, ρ_{490}, ρ_{510}), chlorophyll a (Chl$a$) and attenuation coefficient at 490 nm ($K_d(490)$) in the coastal waters of the North-East Atlantic domain.

Shelf and coastal areas of the domain (i.e., English Channel, ENGC, the Irish Sea, IRIS, the Celtic Sea, CELS, the northwestern British coasts, and the coastal waters of the bay of Biscay, BISC) are characterized by a relatively high contribution of the irregular variations for radiances at 412 nm ($\tilde{\sigma}_I^2$ of 59-67%, and 38% for CELS, Fig. **??**). This is not so in the North Sea (NORS), for which $\tilde{\sigma}_S^2$ reaches 81%. A dominant seasonal cycle is observed for the spectral interval 443-555 nm, particularly for NORS, ENGC, IRIS and CELS, with $\tilde{\sigma}_S^2$ explaining from 69% to 93% of the total variance. For these four regions, $\tilde{\sigma}_S^2$ is only slightly lower for $L_{WN}(670)$. Low values for $\tilde{\sigma}_S^2$ at 412 nm can be partly explained by low values of $L_{WN}(412)$ itself (e.g., Lubac and Loisel, 2007), associated with absorption due to CDOM and non pigmented particles (Tilstone et al., 2005; Vantrepotte et al., 2007). At longer wavelengths, scattering by particles plays a larger role, for instance in the Irish Sea (Bowers et al., 1998). The higher value of $\tilde{\sigma}_S^2$ at 412 nm for the North Sea results from averaging over a large area, where this term is rather high in the central part of the basin and in the Thames River estuary region. Conversely, $\tilde{\sigma}_S^2$ is low for $L_{WN}(412)$ and increases with wavelength in the southern part of the North Sea (German Bight), a region of high phytoplankton production (Joint and Pomroy, 1993) and with an optical interplay of CDOM and particles (e.g., Wild-Allen et al., 2002). Other examples of spatial variability among these regions include a particularly high seasonal component in the northern part of CELS (i.e., just south of Ireland) and low values along the Biscaye slope. The waters downstream of the Thames river (the East Anglian plume, easily seen in satellite images, e.g., Doerffer and Fischer, 1994) are also found with high $\tilde{\sigma}_S^2$ for all wavelengths.

The variability of band ratios is mostly dominated by the seasonal term (Fig.

??). However, $\tilde{\sigma}_S^2$ does not exceed 71% for BISC, and decreases sharply for ENGC, from 88% for $\rho(412)$ to 23% for $\rho(490)$. For $K_d(490)$ and Chl$a$, $\tilde{\sigma}_S^2$ is in the interval 60%-81% and 61%-77%, respectively (except for ENGC, 30 and 33%, respectively). A relatively low seasonal signal for ENGC, and to a lesser extent for BISC, can be related to the combination of factors driving optical properties, including the tidal forcing, sediment re-suspension, or freshwater inputs. Indirectly, variability in these factors also affects the phytoplankton cycle, adding episodic events to the main seasonal signal (e.g., Aiken et al., 2004), or creating conditions leading to variations of this cycle, like late winter blooms (Labry et al., 2001; Gohin et al., 2003).

2.4.2 Trend Analysis

The trend results for the North Atlantic domain are shown by Table 2.4 and Fig. 2.14 to 2.18. It is all the more important to pay attention to the full spatial distribution of trends as some of the Atlantic regions are large: in some cases of heterogeneous trends, the use of regional averages might result in unreliable regional statistics.

	L_{WN}					ρ					
	412	443	490	510	555	412	443	490	510	$K_d(490)$	Chl$a$
North S. (NORS)	-	-	-	-	-	-	0.58*	-	0.23*	-	-
Eng.Chan. (ENGC)	−0.96*	−1.14**	−1.69***	−1.74***	−2.18***	-	0.99**	0.59**	0.54***	−0.67**	−1.30**
Irish S. (IRIS)	−1.27***	−0.87***	−0.91**	−0.88**	−1.14**	-	-	-	0.22*	-	-
Celtic S. (CELS)	-	-	−0.64*	-	−0.88*	-	0.72*	-	0.38**	-	-
Biscay Coast (BISC)	-	-	-	-	−0.99*	1.17**	1.19***	0.64**	0.56***	-	−1.08*
Biscay Off. (BISO)	-	-	-	-	-	1.16**	1.03**	-	0.40*	-	-
Iberian Upw. (IBEU)	-	-	−0.31*	-	-	-	-	-	-	-	-
NW Slope (NWSL)	0.54*	-	-	-	−0.57*	1.38***	1.35**	0.81*	0.76***	-	-
SW Slope (SWSL)	0.83***	0.63***	-	-	−0.63***	1.67***	1.46***	0.82***	0.63***	−0.76**	−1.34**
NE Atl. (NEAT)	0.80**	0.70**	-	-	−0.74**	1.51***	1.46***	0.88***	0.76***	−1.19***	−2.38***
Azores B. (AZORB)	0.96***	0.73***	-	-	−0.55***	1.58***	1.37***	0.79***	0.71***	−1.07***	−2.15***
Norwegian S. (NORW)	-	-	−0.49*	-	−0.45*	-	-	-	-	-	-
Iceland Shelf (ICES)	-	-	-	-	-	0.89*	-	-	-	-	-
Canary Isl. (CANI)	-	-	−0.22**	-	-	-	-	-	-	-	-
Moroccan Upw. (MORU)	−0.49**	−0.36**	−0.33**	-	-	-	-	−0.34*	-	0.59*	-

Student t-test probability : − : NS, * : p<0.05, ** : p<0.01,*** : p<0.001

Table 2.4: Percentage of long term linear changes in SeaWiFS derived radiances (at 412, 443, 490, 510 and 555 nm), band ratios (ρ_{412}, ρ_{443}, ρ_{490}, ρ_{510}), chlorophyll a (Chl$a$) and attenuation coefficient at 490 nm ($K_d(490)$) from November 1997 to October 2007 (in % a^{-1}) in the North-east Atlantic domain. No trend has been detected for the provinces of the Faroe Plateau (FARP) and northwestern British coasts (NWBI). See Fig. 1.4 for a complete definition of the regions.

For the off-shelf domain, trends are detected for the large regions (NWSL, SWSL, NEAT, AZOB). These results are actually due to a large consistent pattern (seen for the various quantities on Fig. 2.14 to 2.18) in the areas VIIk and VIIIe, and the corresponding corners of X and XII. This pattern is associated with a positive trend for L_{WN} at 412, 443 (Fig. 2.14) and 490 nm (lower in the latter case). Conversely, no significant trend is found in that region at 510 nm, whereas the trend is significantly negative at 555 nm (Fig. 2.15). A negative trend at 555 nm is also found in the northern part of XII. Logically, the large pattern of opposite trends for blue and green wavelengths result in large and highly significant positive signals for band ratios (Fig. 2.16). For the regions NWSL, SWSL, NEAT, and AZOB, the trends of $\rho(412)$ and $\rho(443)$ amount to approximately +1.5% a^{-1} (Table 2.4). Correspondingly, large negative trends are observed for $K_d(490)$ and Chl$a$ (Fig. 2.17 and 2.18). Opposite to these features, opposite trends are found for L_{WN} between 412 and 490 nm in the southern part of IXb (decrease) and for $L_{WN}(555)$ in VIb (increase), associated with negative trends in $\rho(443)$ (Fig. 2.16).

Other isolated features include a decrease in L_{WN} in the blue domain in the northern part of the Moroccan upwelling (MORU) as well as an increase west of Iceland, and a decrease of $L_{WN}(555)$ in the southeast of the Norwegian Sea (along the coasts of Norway) (Fig. 2.15). Positive and negative signals can be observed for $\rho(443)$ (Fig. 2.16) west and along the southeastern shores of Iceland, respectively. Trends can be also found for $\rho(443)$ along the northern Moroccan coasts (MORU) (<0) and in the Gulf of Cádiz (in the area IBEU, or IXa) probably in response to local variations in upwelling and river discharge (Navarro and Ruiz, 2006). The trends are obviously reversed for $K_d(490)$ and Chl$a$ (Fig. 2.17 and 2.18).

For the shelf regions, a couple of interesting patterns appear. Particularly, a negative trend is found for L_{WN} at all wavelengths for IRIS and ENGC as well as in CELS at the southwestern tip of England. The trend in the English Channel mostly affects the western part and increases with wavelength (reaching -2.2% a^{-1} for the area averaged series at 555 nm). In the North Sea, negative trends are also seen for L_{WN} along the Dutch coasts and downstream of the Thames River. Averaged over the whole NORS area, these trends are not significant (Table 2.4). Finally a negative signal for $L_{WN}(555)$ affects some offshore parts of NORS and the French coasts of the Bay of Biscaye (-1% a^{-1} for the area averaged series). As for band ratios, trends are mostly positive, in the English Channel (but of lower amplitude than for L_{WN}), the open North Sea, the French coasts of the Bay of Biscaye (+1.2% a^{-1} for $\rho(443)$ and BISC), and isolated patterns north and south of Ireland (Fig. 2.12). Consequently, satellite derived $K_d(490)$ and Chl$a$ tend to decrease for these regions. These results for the central North Sea are consistent with those of McQuatters-Gollop et al. (2007), showing a decrease between 1998 and 2003 of Chl$a$ obtained by combining Continuous Plankton Recorder (CPR) and SeaWiFS data (the decrease being actually continuous since 2000). Conversely, no significant trends in ratios are found for the German Bight, a result in continuity with the coastal series of McQuatters-Gollop et al. (2007) over the SeaWiFS period, the Chl$a$ observations over 1988-1995 of de Vries et al. (1998) for the Dutch coastal waters (in spite of a decrease in phosphorus load), and the work of Cadée and Hegeman (2002) who show that after an increase in the 1970's, the annual Chl$a$ was stable in the 1990's at a coastal station of the Wadden Sea. Edwards et al. (2006) have illustrated an increase in abundance of some dinoflagellate taxa along the coasts of southern Norway, including the area of positive trend for $\rho(443)$ seen on Fig. 2.12, between the 1990's and the preceding period, but this

record has been fluctuating over the interval 1997-2002. The different results obtained for some off-shelf waters (opposite trends for blue and green wavelengths) and the English Channel (negative trends for all $L_{WN}(\lambda)$) underline the information brought by the full L_{WN} spectrum. The latter might be interpreted as a relative decrease in the load of scattering particles in the water column, driven by variability in river run-off and/or wind regime. The off-shelf waters are closer to Case-1 conditions with phytoplankton and derived elements driving the optical properties, and consequently clearer variations of the blue-to-green band ratios.

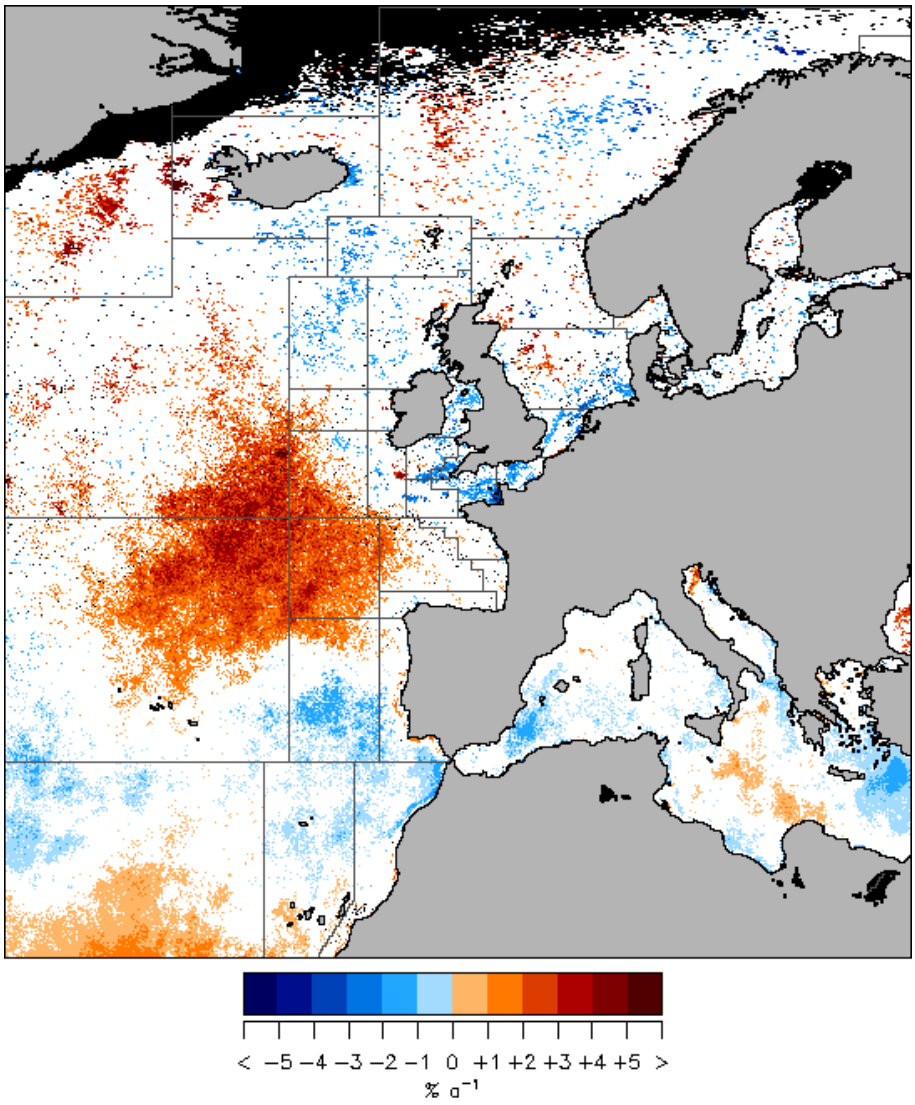

Figure 2.14: Relative linear changes in $L_{WN}(443)$ over the 10-year SeaWiFS record (from November 1997 to October 2007, in % a^{-1}) in the North east Atlantic domain and in the Baltic Sea. Only the pixels for which a significant linear trend has been detected are reported ($p < 0.05$).

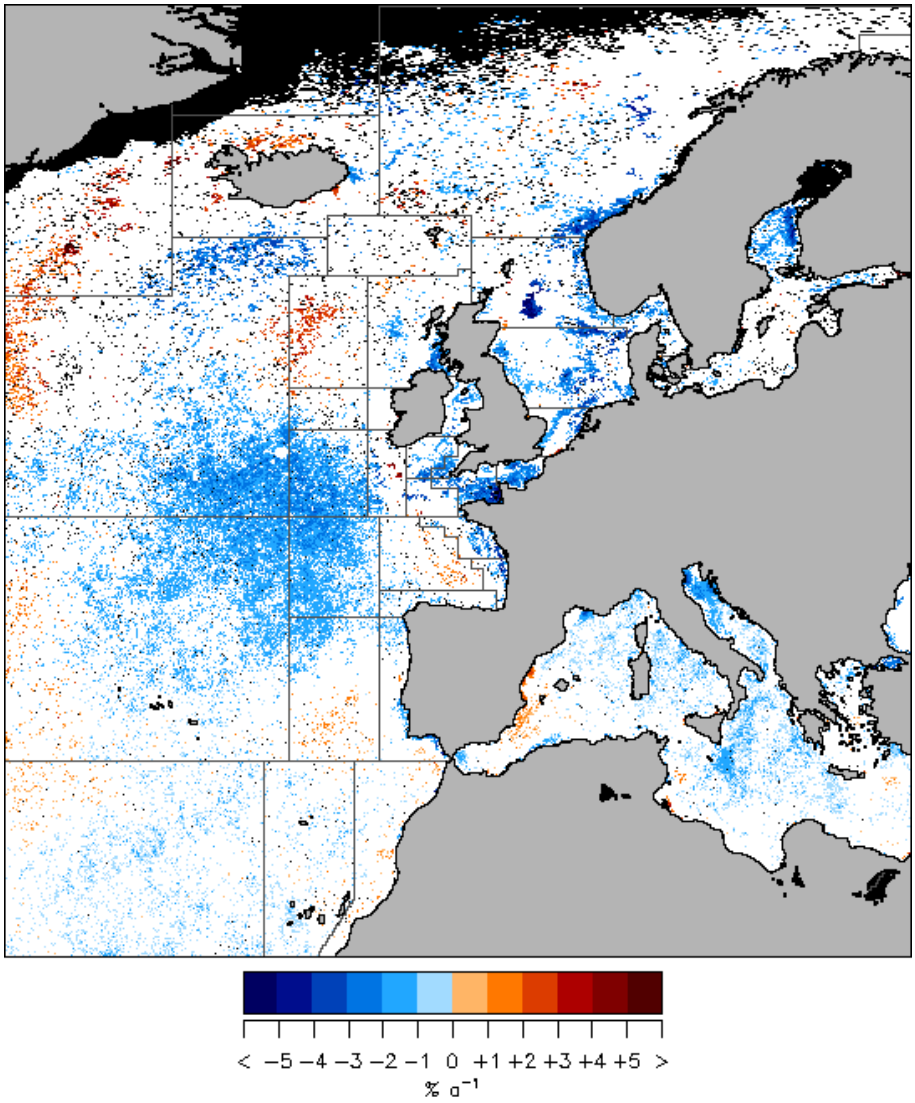

Figure 2.15: Relative linear changes in $L_{WN}(555)$ over the 10-year SeaWiFS record (from November 1997 to October 2007, in % a^{-1}) in the North east Atlantic domain and in the Baltic Sea. Only the pixels for which a significant linear trend has been detected are reported ($p < 0.05$).

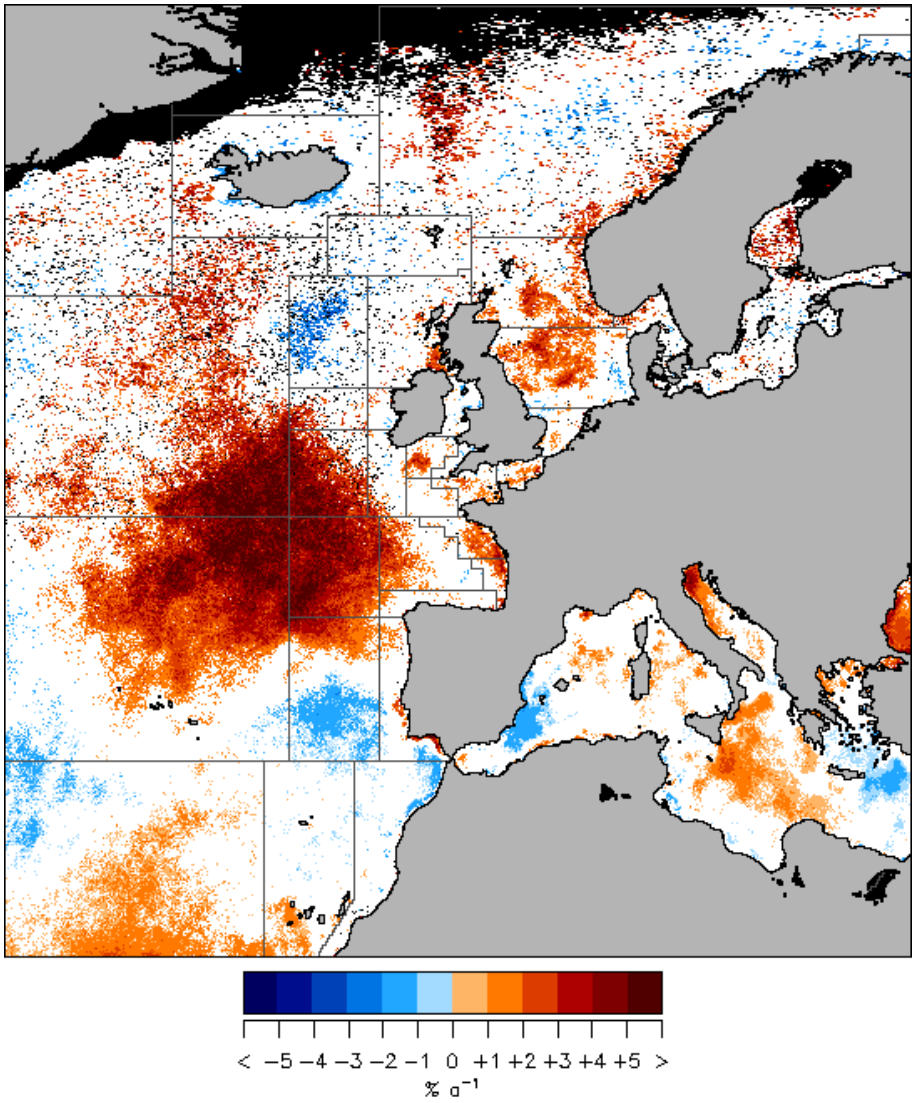

Figure 2.16: Relative linear changes in the band ratio $\rho(443)$ over the 10-year SeaWiFS record (from November 1997 to October 2007, in % a^{-1}) in the North east Atlantic domain and in the Baltic Sea. Only the pixels for which a significant linear trend has been detected are reported ($p < 0.05$).

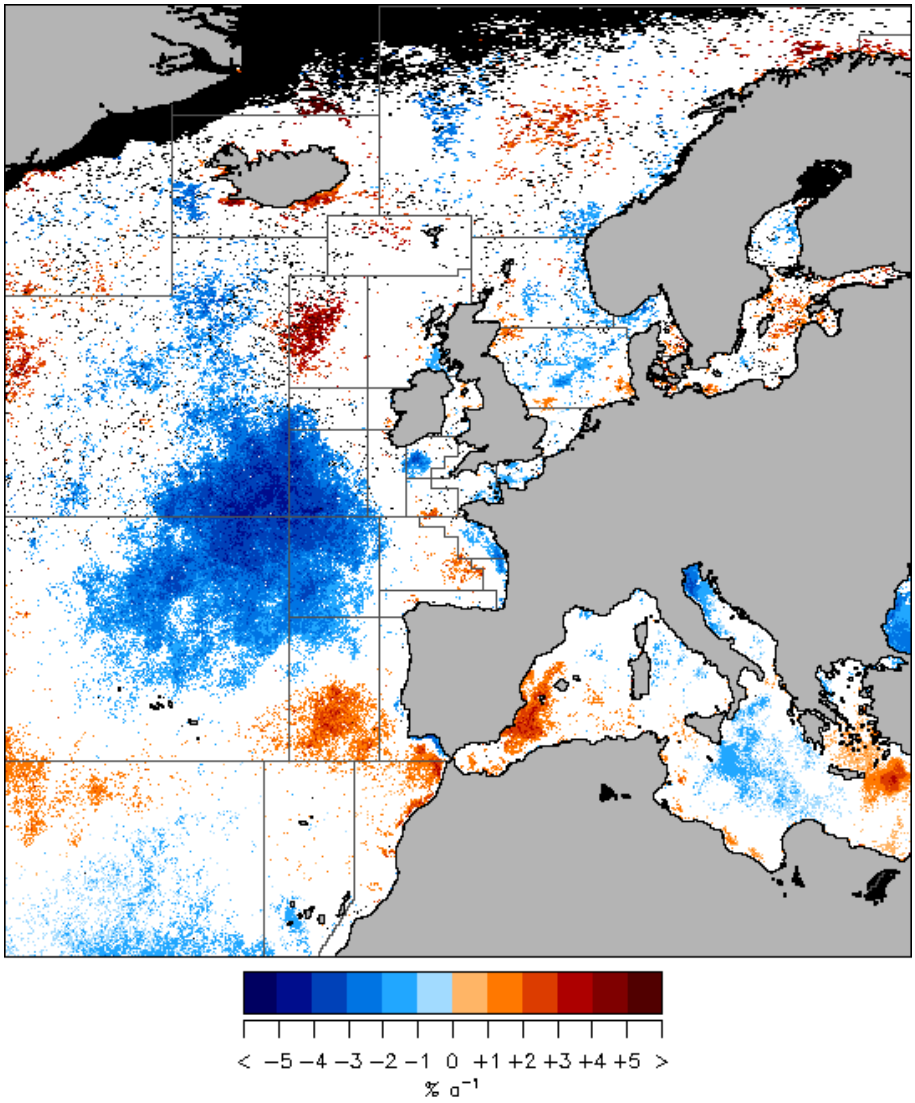

Figure 2.17: Relative linear changes in the diffuse attenuation coefficient $K_d(490)$ over the 10-year SeaWiFS record (from November 1997 to October 2007, in % a^{-1}) in the North east Atlantic domain and in the Baltic Sea. Only the pixels for which a significant linear trend has been detected are reported ($p < 0.05$).

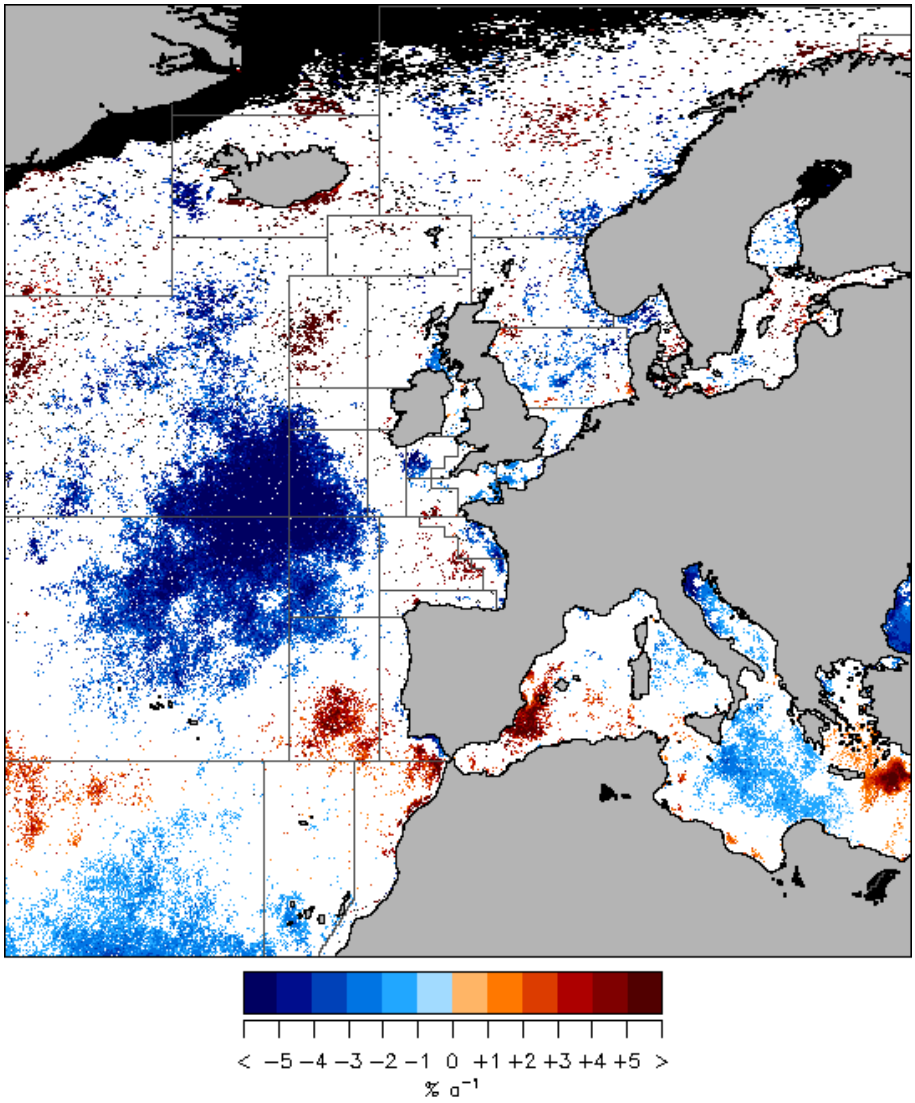

Figure 2.18: Relative linear changes in the chlorophyll *a* concentration Chl*a* over the 10-year SeaWiFS record (from November 1997 to October 2007, in % a^{-1}) in the North east Atlantic domain and in the Baltic Sea. Only the pixels for which a significant linear trend has been detected are reported ($p < 0.05$).

An abundant literature has highlighted the regime shift affecting the North Sea and northeastern North Atlantic ecosystems (west of western Europe) in the mid 1980's, with an abrupt increase in phytoplankton biomass (e.g., Reid et al., 1998; Raitsos et al., 2005), and changes in several trophic levels up to fish (Beaugrand and Reid, 2003). Particularly, these took the form of a northward extension of warm water species, documented for zooplankton and fish (Beaugrand et al., 2002; Beare et al., 2004; Perry et al., 2005), variations in phenology (Edwards and Richardson, 2004) and community structure (Leterme al., 2006), or increases in jellyfish abundance (Attrill et al., 2005). Continuous monitoring is necessary to be able to detect similar changes in the future and in any case a departure from the warm biological dynamic regime 1984-1999 (Beaugrand and Ibañez, 2004). In that respect, it is interesting to see that the trends detected west of western Europe (Fig. 2.16 to 2.18) seems opposite to the large increases in phytoplankton in the late 1980's. Changes affecting the North Sea and Northeast Atlantic have been diversely related to the North Atlantic Oscillation (NAO, see Drinkwater et al., 2003, for reviews), that entered a period of strong positive index in the 1980's (Hurrell, 1995). Oscillations of the NAO index in a more neutral state over the last few years might partly be related to the observed trend in color. A final comment refers to the study of Antoine et al. (2005), who processed Coastal Zone Color Scanner (1978-1986) and SeaWiFS data in a consistent manner. The resulting comparison revealed an increase in Chl$a$ between the two periods in a location strikingly similar to that shown for $\rho(443)$ in the Atlantic offshore western Europe, again consistent with a reversal of past trends. Clearly, the continuation of monitoring effort is a prerequisite to detect the coming changes in these regional ecosystems, as they undergo the fluctuations in climate, variations in sea surface temperature (Good et al., 2007; Gómez-Gesteira et al., 2008), or in water masses (Leterme al., 2008), as well as in coastal regions the variability in inputs from land or the threat of invasive species (e.g., Faasse and Bayha, 2006).

Section 3

Discussion and Conclusions

This study has attempted a description of the space and time variability of the monthly SeaWiFS record of normalized water leaving radiance over the European marine macro-region. The standard derived products, $K_d(490)$ and Chl$a$, have also been considered for completeness, but the uncertainties associated with these products in marginal seas and coastal waters (particularly for Chl$a$) warrants caution. The synoptic coverage afforded by satellite remote sensing has been summarized by average time series on a set of regions partitioning the domain. Overall, the results obtained on a grid-point basis are found consistent even if departures have been mentioned, particularly for the northern part of the Atlantic domain. The fact that in general $\tilde{\sigma}_S^2$ for a given grid-point is lower than for the area averaged series was to be expected; besides the reduction of noise by the averaging process and possible artifacts due to cloud coverage for northern regions, an analysis performed on a fixed point is restricted to an eulerian framework.

The results shown on Fig. 2.1 to 2.18 are synthesized by a classification of the European regions according to the relative contributions of seasonal, irregular and trend terms to the total variance, as shown on Fig. 3.1 for four representative variables (L_{WN} at 443 and 555 nm, $\rho(443)$ and $K_d(490)$). The two axes of each graph represent $\tilde{\sigma}_S^2$ and $\tilde{\sigma}_I^2$, and the distance from the point to the dashed diagonal (going parallel to the axes) quantifies $\tilde{\sigma}_T^2$. It is recalled that here $\tilde{\sigma}_S^2$ only pertains to a strictly periodic seasonal cycle. Fig. 3.1 clearly emphasizes the high heterogeneity existing in the characteristics of temporal variability for the marine optical properties in the various European waters. The highly seasonal time series found for the radiance signal and band ratios in the blue part of the spectrum (i.e., $L_{WN}(443)$ and $\rho(443)$) for the Mediterranean Sea strongly contrast with those, strongly irregular, observed in the Baltic and in the Black Sea (western part). Similarly, the percentages of variance corresponding to the two latter domains are globally more dispersed than the data of the Mediterranean Sea which appears to be much more optically homogeneous (except the north Adriatic data). This reflects the differences existing in the environmental parameters driving the quality of these water masses (like terrestrial inputs and marine biological activity). In terms of derived products such as Chl$a$, it is argued here that the low variance associated with the seasonal component for AOPs in the Baltic Sea underlines the difficulty of accurately extracting the seasonal cycle of phytoplankton biomass from the ocean color record.

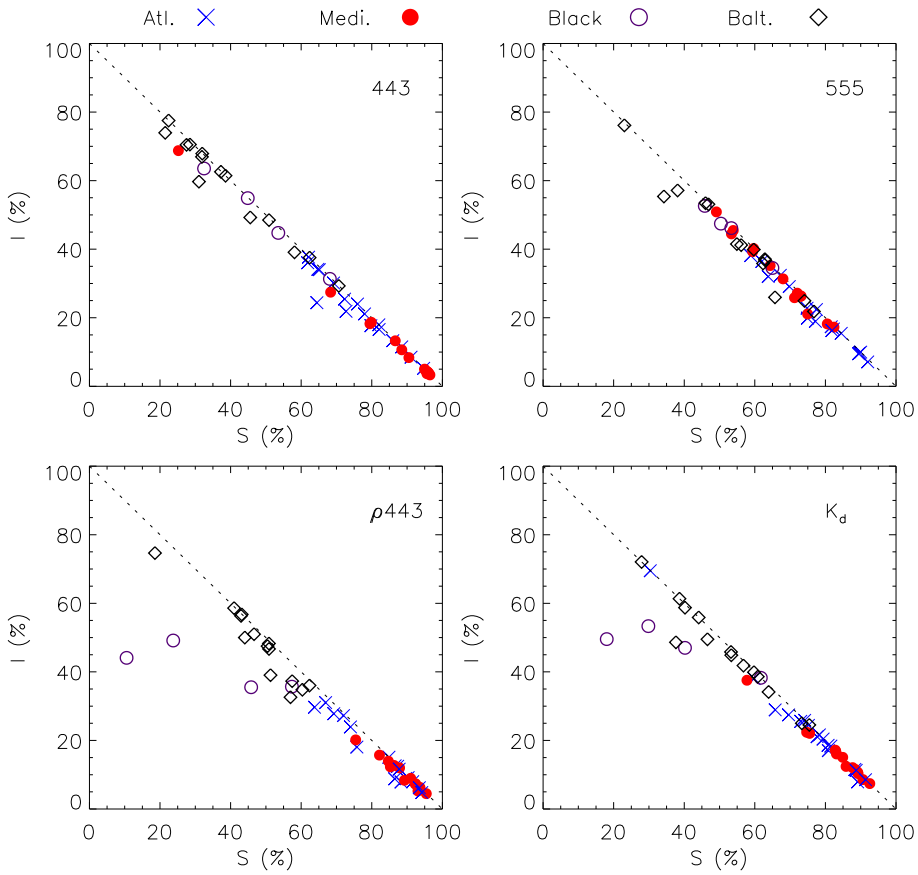

Figure 3.1: Relative contribution (in %) of the seasonal ($\tilde{\sigma}_S^2$), irregular ($\tilde{\sigma}_I^2$) and trend ($\tilde{\sigma}_T^2$) components to the total variance of the time series for SeaWiFS L_{WN} at 443 and 555 nm, the band ratio ρ_{443} and the attenuation coefficient at 490 nm ($K_d(490)$) in the European waters.

A linear trend affecting the optical characteristics of the water has been found for different regions of the European seas. These include the Atlantic Ocean west of the European western shelf, the central North Sea, the English Channel, the Black Sea, the northern Adriatic, various regions of the Mediterranean Sea and the northern Baltic. Profound changes are likely to affect the European marine ecosystems, and thus their optically significant constituents. In coastal waters, variations in precipitation and river flow, as well as retention by dams, and the varying intensity of re-suspension from the bottom impact the concentrations of inorganic particles and CDOM. The different trophic levels, including phytoplankton, undergo a complex interplay of pressures, including climate variability, the effect of which has been mentioned in several occasions in the preceding sections, the emergence of invasive species and diseases (Carlton and Geller, 1993; Harvell et al., 1999), overfishing with its potential top-down impacts (e.g., Frank et al., 2005), and variations in inputs of nutrients and contaminants. In that context northern European waters have been classified as highly to very highly impacted by human activities (Halpern et al., 2008). The variations in L_{WN} are ultimately the visual manifestation of these changes when they affect optically significant constituents.

Even though references have been provided to tentatively relate the present description to documented analyzes of field observations, it is out of the scope of this work to explain how the various optically significant constituents in the water drive the variability in L_{WN} at the scale of the European seas, nor to understand the various trends that have been detected. This principally requires a set of bio-optical algorithms deriving the appropriate products for the different European regions with quantified uncertainties. Moreover, reference long time series of optical properties describing the contributions of phytoplankton, non-pigmented particles and DOM to the light field would be important in order to validate the trends obtained by the satellite products, but such data sets are likely to remain very few. Conversely, the creation of consistent records of continuous measurements of L_{WN} has been achieved in recent years (Zibordi et al., 2006b). In any case, the importance of quantifying the concentrations of optically significant constituents does not lessen that of monitoring L_{WN} per se. The color of the water has long been considered as a precious indicator of water quality, from the time of the Forel-Ule color scale (Arnone et al., 2004), and is now considered an Essential Climate Variable (GCOS, 2006). The present work took advantage of a decade-long series derived from one sensor but continuous monitoring will require a multi-platform approach, a work in progress considering the differences between sensor products (e.g., Mélin et al., 2008). Constructing and maintaining a fully consistent record of L_{WN} is thus a high priority.

Acknowledgements

The authors would like to thank the Ocean Biology Processing Group of NASA for the distribution of the SeaWiFS L1A data. We also thank Pr. Frédéric Ibanez for his help on the eigenvector filtering method.

Bibliography

Aiken, J., Fishwick, J., Moore, G., Pemberton, K., 2004. The annual cycle of phytoplankton photosynthetic quantum efficiency, pigment composition and optical properties in the western English Channel. Journal of the Marine Biological Association of the U.K., 84, 301-313.

Alheit, J., Möllmann, C., Dutz, J., Kornilovs, G., Loewe, P., Mohrholz, V., Wasmund, N., 2005. Synchronous ecological regime shifts in the central Baltic and the North Sea in the late 1980s. ICES Journal of Marine Science, 62, 1205-1215.

Antoine, D., Morel, A., Gordon, H.R., Banzon, V.F., Evans, R.H., 2005. Bridging ocean color observations of the 1980s and 2000s in search of long-term trends. Journal of Geophysical Research, 110, C06009, 10.1029/2004JC002620.

Arnone, R.A., Wood, A.M., Gould, R.W., 2004. The evolution of optical water mass classification. Oceanography, 17, 14-15.

Attrill, M.J., Wright, J., Edwards, M., 2007. Climate-related increases in jellyfish frequency suggest a more gelatinous future for the North Sea. Limnology and Oceanography, 52, 480-485.

Beare, D.J., Burns, F., Greig, A., Jones, E.G., Peach, K., Kienzle, M., McKenzie, E., Reid, D.G., 2004. Long-term increases in prevalence of North Sea fishes having southern biogeographic affinities. Marine Ecology Progress Series, 284, 269-278.

Beaugrand, G., Reid, P.C., Ibañez, F., Lindley, J.A., Edwards, M., 2002. Reorganization of North Atlantic marine copepod biodiversity and climate. Science, 296, 1692-1694.

Beaugrand, G., Reid, P.C., 2003. Long-term changes in phytoplankton, zooplankton and salmon related to climate. Global Change Biology, 9, 801-817.

Beaugrand, G., Ibañez, F., 2004. Monitoring marine plankton ecosystems. II. Long-term changes in North Sea calanoid copepods in relation to hydro-climatic variability. Marine Ecology Progress Series, 284, 35-47.

Bernardi Aubry, F., Berton, A., Bastianini, M., Socal, G., Acri, F., 2004. Phytoplankton succession in a coastal area of the NW Adriatic, over a 10-year sampling period (1990-1999). Continental Shelf Research, 24, 97-115.

Berthon, J.-F., Mélin, F., Zibordi, G., 2008. Ocean colour remote sensing of the optically complex European seas. In "Remote Sensing of the European Seas", Eds Barale, V., & Gade, M., Springer, pp.35-52.

Bignami, F., Sciarra, R., Carniel, S., Santoleri, R., 2007. Variability of Adriatic Sea coastal turbid waters from SeaWiFS imagery. Journal of Geophysical Research, 112, C03S10, 10.1029/2006JC003518.

Blondeau-Patissier, D., Tilstone, G.H., Martinez-Vicente, V., Moore, G.F., 2004. Comparison of bio-physical marine products from SeaWiFS, MODIS and a bio-optical model with in situ measurements from Northern European waters. Journal of Optics A: Pure & Applied Optics, 6, 875-889.

Bowers, D.G., Boudjelas, S., Harker, E.L., 1998. The distribution of fine suspended sediments in the surface waters of the Irish Sea and its relation to tidal stirring. International Journal of Remote Sensing, 19, 2789-2805.

Bricaud, A., Bosc, E., Antoine, D., 2002. Algal biomass and sea surface temperature in the Mediterranean basin. Intercomparison of data from various satellite sensors, and implications for primary production estimates. Remote Sensing of Environment, 81, 163-178.

Cadée, G.C., Hegeman, J., 2002. Phytoplankton in the Marsdiep at the end of the 20th century; 30 years of monitoring biomass, primary production, and Phaeocystis blooms. Journal of Sea Research, 48, 97-110.

Carlton, J.T., and Geller, J.B., 1993. Ecological roulette: The global transport of non-indigeneous marine organisms. Science, 261, 78-82.

Carstensen, J., Conley, D.J., Henriksen, P., 2004. Frequency, composition, and causes of summer phytoplankton blooms in a shallow coastal ecosystem, the Kattegat. Limnology and Oceanography, 49, 190-201.

Clark G.L., Ewing, G.C., Lorenzen, C.J., 1970. Spectra of backscattered light from the sea obtained from aircraft as a measure of chlorophyll concentration. Science, 167, 1119-1121.

Claustre, H., Fell, F., Oubelkheir, K., Prieur, L., Sciandra, A., Gentili, B., Babin, M., 2000. Continuous monitoring of surface optical properties across a geostrophic front: Biogeochemical inferences. Limnology and Oceanography, 45, 309-321.

Cokacar, T., Oguz, T., Kubilay, N., 2004. Satellite-detected early summer coccolithophore blooms and their interannual variability in the Black Sea. Deep-Sea Research, I, 1017-1031.

COM (2002) 539. Towards a strategy to protect and conserve the marine environment. Communication from the Commission to the Council and the European Parliament, 2002.

COM (2005) 504. Thematic strategy on the protection and conservation of the marine environment. Communication from the Commission to the Council and the European Parliament, 2005.

Darecki, M., Weeks, A., Sagan, S., Kowalczuk, P., Kaczmarek, S., 2003. Optical characteristics of two contrasting Case 2 waters and their influence on remote sensing algorithms. Remote Sensing of Environment, 23, 237-250.

Darecki, M., Stramski, D., 2004. An evaluation of MODIS and SeaWiFS bio-optical algorithms in the Baltic Sea. Remote Sensing of Environment, 89, 326-350.

Daskalov, G.M., 2002. Overfishing drives a trophic cascade in the Black Sea. Marine Ecology Progress Series, 225, 53-63.

de Vries, I., Duin, R.N.M., Peeters, J.C.H., Los, F.J., Bokhorst, M., Laane, R.W.P.M., 1998. Patterns and trends in nutrients and phytoplankton in Dutch coastal waters: Comparison of time series analysis, ecological model simulation, and mesocosm experiments. ICES Journal of Marine Science, 55, 620-634.

Doerffer, R., Fischer, J., 1994. Concentration of chlorophyll, suspended matter, and gelbstoff in case II waters derived from satellite coastal zone color scanner. Journal of Geophysical Research, 99, 7457-7466.

D'Ortenzio, F., Ragni, M., Marullo, S., Ribera d'Alcal, M., 2003. Did biological activity in the Ionian Sea change after the Eastern Mediterranean Transient? Results from the analysis of remote sensing observations. Journal of Geophysical Research, 108, 8113, 10.1029/2002JC001556.

Drinkwater, K.F., Belgrano, A., Borja, A., Convsersi, A., Edwards, M., Greene, C.H., Ottersen, G., Pershing, A.J., Walker, H., 2003. The response of marine ecosystems to climate variability associated with the North Atlantic Oscillation. In "The North Atlantic Oscillation: Climate significance and enviromental impact". Eds., J.W. Hurrell, Y. Kushnir, G. Ottersen, M. Visbeck, Geophysical Monograph Series of the American Geophysical Union, 134, 211-234.

Edwards, M., Richardson, A.J., 2004. Impact of climate change on marine pelagic phenology and trophic mismatch. Nature, 430, 881-884.

Edwards, M., Johns, D.G., Leterme, S.C., Richardson, A.J., 2006. Regional climate change and harmful algal blooms in the northeast Atlantic. Limnology and Oceanography, 51, 820-829.

Faasse, M.A., Bayha, K.M., 2006. The ctenophore *Mnemiopsis leidyi* A. Agassiz 1865 in coastal waters of the Netherlands: An unrecognized invasion? Aquatic Invasions, 1, 270-277.

Ferrari, G.M., Dowell, M.D., Grossi, S., Targa, C., 1996. Relationship between the optical properties of chromophoric dissolved organic matter and total concentration of dissolved organic carbon in the southern Baltic Sea region. Marine Chemistry, 55, 299-316.

Findley, D.F., Monsell, B.C., Bell, W.R., Otto, M.C., Bor-Chung, C., 1998. New Capabilities and Methods of the X-12-ARIMA Seasonal-Adjustment Program. Journal of Business and Economic Statistics, 16, 122-177.

Fleming, V., Kaitala, S., 2006. Phytoplankton spring bloom intensity index for the Baltic Sea estimated for the years 1992 to 2004. Hydrobiologia, 554, 57-65.

Fleming-Lehtinen, V., Laamanen, M., Kuosa, H., Haahti, H., Olsonen, R., 2008. Long-term development of inorganic nutrients and chlorophyll *a* in the open northern Batic Sea. Ambio, 37, 86-92.

Frank, K.T., Petrie, B., Choi, J.S., Leggett, W.C., 2005. Trophic cascades in a formerly cod-dominated ecosystem. Science, 308, 1621-1623.

Gabric, A.J., Garcia, L., Van Camp, L., Nykjaer, L., Eifler, W., Schrimpf, W., 1993. Offshore export production in the Cape Blanc (Mauritania) gian filament as derived from Coastal Zone Color Scanner imagery. Journal of Geophysical Research, 98, 4697-4712.

Garçon, V., Oschlies, A., Doney, S.C., McGillicuddy, D., Waniek, J., 2001. The role of mesoscale variability on plankton dynamics in the North Atlantic. Deep-Sea Research, II, 48, 2199-2226.

GCOS, Report GCOS-107. Systematic observation requirements for satellite-based products for climate, in "Implementation Plan for the Global Observing System for Climate in Support of the UNFCCC - Supplemental details to the satellite-based component", WMO/TD No. 1338, 103pp., 2006.

Ginzburg, A.I., Kostianoy, A.G., Sheremet, N.A., 2004. Seasonal and interannual variability of the Black Sea surface temperature as revealed from satellite data (1982-2000). Journal of Marine Systems, 52, 33-50.

Goffart, A., Hecq, J.-H., Legendre, L, 2002. Changes in the development of the winter-spring phytoplankton bloom in the Bay of Calvi (NW Mediterranean) over the last two decades: A response to changing climate? Marine Ecology Progress Series, 236, 45-60.

Gohin, F., Lampert, L., Guillaud, J.-F., Herbland, A., Nézan, E., 2003. Satellite and in situ observations of a late winter phytoplankton bloom, in the northern Bay of Biscay. Continental Shelf Research, 23, 1117-1141.

Gómez-Gesteira, M., de Castro, M., Alvarez, I., Gómez-Gesteira, J.L., 2008. Coastal sea surface temperature warming trend along the continental part of the Atlantic arc (1985-2005). Journal of Geophysical Research, 113, C04010, 10.1029/2007JC004315.

Good, S.A., Corlett, G.K., Remedios, J.J., Noyes, E.J., Llewellyn-Jones, D.T., 2007. The global trend in sea suface temperature from 20 years of Advanced Very High Resolution Radiometer data. Journal of Climate, 20, 1255-1264, 2007.

Gordon H.R., Wang, M., 1994. Retrieval of water-leaving radiance and aerosol optical thickness over the oceans with SeaWiFS: a preliminary algorithm. Applied Optics, 33, 443-452.

Halpern, B.S., Walbridge, S., Selkoe, K.A., Kappel, C.V., Michelo, F., D'Agrosa, C., Bruno, J.F., Casey, K.S., Ebert, C., Fox, H.E., Fujita, R., Heinemann, D., Lenihan, H.S., Madin, E.M.P., Perry, M.T., Selig, E.R., Spalding, M., Steneck, R., Watson, R., 2008. A global map of human impact on marine ecosystems. Science, 319, 948-952.

Hansen, B., Eliasen, S.K., Gaard, E., Larsen, K.M.H., 2005. Climatic effects on plankton and productivity on the Faroe Shelf. ICES Journal of Marine Science, 62, 1224-1232.

Harvell, C.D., Kim, K., Burkholder, J.M., Colwelll, R.R., Epstein, P.R., Grimes, D.J., Hofman, E.E., Lipp, E.K., Osterhaus, A.D.M.E., Overstreet, R.M., Porter, J.W., Smith, G.W., Vasta, G.R., 1999. Emerging marine diseases - Climate links and anthropogenic factors. Science, 285, 1505-1510.

Haslob, H., Clemmesen, C., Schaber, M., Hinrichsen, H.-H., Schmidt, J.O., Voss, R., Kraus, G., Köster, F.W., 2007. Invading *Mnemiopsis leidyi* as a potential threat to Baltic fish. Marine Ecological Progress Series, 349, 303-306.

HELCOM, 2007b. Climate change in the Baltic Sea area - HELCOM Thematic Assessment in 2007. Baltic Sea Environment Proceedings No. 111.

HELCOM, 2007a. HELCOM Baltic Sea Action Plan - Ministerial Meeting, Nov. 2007, Krakow, Poland, 101pp.

Højerslev, N.K., 1989. Surface water quality studies in the interior marine environment of Denmark. Limnology and Oceanography, 34, 1630-1639.

Hooker, S.B., Esaias, W.E., Feldman, G.C., Gregg, W.W., McClain, C.R., 1992. An overview of SeaWiFS and ocean color. *NASA Technical Memorandum, 1992-104566, vol. 1*, 1-24, Eds., S.B. Hooker, & E.R. Firestone, NASA-GSFC, Greenbelt, Maryland.

Humborg, C., Ittekkot, V., Cociasu, A., Bodungen, B., 1997. Effect of Danube River dam on Black Sea biogeochemistry and ecosystem structure. Nature, 386, 385-388.

Hurrell, J.W., 1995. Decadal trends in the North Atlantic Oscillation: Regional temperatures and precipitation. Science, 269, 676–679.

Ibanez, F., Conversi, A., 2002. Prediction of missing values and detection of 'exceptional events' in a chronological planktonic series: a single algorithm. Ecological Modelling, 154, 9-23.

Janssen, F., Neumann, T., Schmidt, M., 2004. Inter-annual variability in cyanobacteria blooms in the Baltic Sea controlled by wintertime hydrographic conditions. Marine Ecology Progress Series, 275, 59-68.

Jevrejeva, S., Drabkin, V.V., Kostjukov, J., Lebedev, A.A., Lepäranta, M., Mironov, Ye. U., Schmelzer, N., Sztobryn, M., 2004. Baltic Sea ice seasons in the twentieth century. Climate Research, 25, 217-227.

Joint, I., Pomroy, A., 1993. Phytoplankton biomass and production in the southern North Sea. Marine Ecology Progress Series, 99, 169-182.

Kahru, M., Savchuk, O.P., Elmgren, R., 2007. Satellite measurements of cyanobacterial bloom frequency in the Baltic Sea: Interannual and spatial variability. Marine Ecology Progress Series, 343, 15-23.

Karabashev, G.S., Sheberstov, S.V., Yakubenko, V.G., 2006. The June maximum of normalized radiance and its relation to the hydrological conditions and coccolithophorid bloom in the Black Sea. Oceanology, 46, 305-317.

Karageorgis, A.P., Gardner, W.D., Georgopoulos, D., Mishonov, A.V., Krasakopoulou, E., Anagnostou, C., 2008. Particle dynamics in the eastern Mediterranean Sea: A synthesis based on light transmission, PMC, and POC archives (1991-2001). Deep-Sea Research, I, 55, 177-202.

Kideys, A.E., Romanova, Z., 2001. Distribution of gelatinous macrozooplankton in the southern Black Sea during 1996-1999. Marine Biology, 139, 535-547.

Kideys, A.E., 2002. Fall and rise of the Black Sea ecosystem. Science, 297, 1482-1484.

Kideys, A.E., Roohi, A., Bagheri, S., Finenko, G., Kamburska, L., 2005. Impacts of invasive ctenophores on the fisheries of the Black Sea and Caspian Sea. Oceanography, 18, 76-85.

Konovalov, S.K., Murray, J.W., 2001. Variations in the chemistry of the Black Sea on a time scale of decades (1960-1995). Journal of Marine Systems, 31, 217-243.

Kopelevich, O.V., Sheberstov, S.V., Yunev, O., Basturk, O., Finenko. Z.Z., Nikonov, S., Vedernikov, V.I., 2002. Surface chlorophyll in the Black Sea over 1978-1986 derived from satellite and in situ data. Journal of Marine Systems, 36, 145-160.

Kutser, T., 2004. Quantitative detection of chlorophyll in cyanobacterial blooms by satellite remote sensing. Limnology and Oceanography, 49, 2179-2189.

Labry, C., Herbland, A., Delmas, D., Laborde, P., Lazure, P., Froidefond, J.-M., Jegou, A.M., Sautour, B., 2001. Initiation of winter phytoplankton blooms within the Gironde plume waters in the Bay of Biscay. Marine Ecology Progress Series, 212, 117-130.

Lefèvre, D., Minas, H.J., Robinson, M., Williams, P.J. le B., Woodward, E.M.S., 1997. Review of gross community production, primary production, net community production and dark community respiration in the Gulf of Lions. Deep-Sea Research, II, 44, 801-832.

Leterme, S., Seuront, L., Edwards, M., 2006. Differential contribution of diatoms and dinoflagellates to phytoplankton biomass in the NE Atlantic Ocean and the North Sea. Marine Ecology Progress Series, 312, 57-64.

Leterme, S.C., Pingree, R.D., Skogen, M.D., Seuront, L., Reid, P.C., Attrill, M.J., 2008. Decadal fluctuations in North Atlantic water inflow in the North Sea between 1958-2003: Impacts on temperature and phytoplankton populations. Oceanologia, 50, 59-72.

Lévy, M., Mémery, L., Madec, G., 1999. The onset of the spring bloom in the MEDOC area: Mesoscale spatial variability. Deep-Sea Research, I, 1137-1160.

Longhurst, A.R., 1998. Ecological Geography of the Sea. San Diego: Academic Press, 398pp.

Lubac, B., Loisel, H., 2007. Variability and classification of remote sensing reflectance spectra in the eastern English Channel and southern North Sea. Remote Sensing of Environment, 110, 45-58.

Makridakis, S.G., Wheelwright, S.C., McGee, V.E., 1998. Forecasting: Methods and Applications. 3rd ed. Wiley, New York, 656pp.

Marty, J.-C., Chiavérini, J., Pizay, M.-D., Avril, B., 2002. Seasonal and interannual dynamics of nutrients and phytoplankton pigments in the western Mediterranean Sea at the DYFAMED time-series station (1991-1999). Deep-Sea Research, II, 49, 1965-1985.

Mauri, E., Poulain, P.-M., Južnič-Zonta, Ž.: MODIS chlorophyll variability in the northern Adriatic Sea and relationship with forcing parameters. Journal of Geophysical Research, 112, C03S11, 10.1029/2006JC003545.

McClain, C.R., Signorini, S.R., Christian, J.R., 2004. Subtropical gyre variability observed by ocean-color satellites. Deep-Sea Research, II, 51, 281-301.

McKee, D., Cunnigham, A., Dudek, A., 2007. Optical water type discrimination and tuning remote sensing band-ratio algorithms: Application to retrieval of chlorophyll and $K_d(490)$ in the Irish and Celtic Seas. Estuarine Coastal and Shelf Science, 73, 827-834.

McQuatters-Gollop, A., Raitsos, D.E., Edwards, M., Pradhan, Y., Mee, L.D., Lavender, S.J., Attrill, M.J., 2007. A long-term chlorophyll data set reveals regime shift in North Sea phytoplankton biomass unconnected to nutrient trends. Limnology and Oceanography, 52, 635-648.

Meier, H.E.M., Döscher, R., Halkka, A., 2004. Simulated distributions of Baltic Sea ice in warming climate and consequences for the winter habitat of the Baltic ringed seal. Ambio, 33, 249-256.

Mélin, F., Zibordi, G., Berthon, J.-F., 2007. Assessment of satellite ocean color products at a coastal site. Remote Sensing of Environment, 110, 192-215.

Mélin, F., Zibordi, G., Djavidnia, S., 2008. Merged series of normalized water leaving radiances obtained from multiple satellite missions for the Mediterranean Sea. Advances in Space Research, 10.1016/j.asr.2008.04.004.

Morel, A., Maritorena, S., 2001. Bio-optical properties of oceanic waters: A reappraisal. Journal of Geophysical Research, 106, 7163-7180.

Morel, A., Antoine, D., Gentili, B., 2002. Bidirectional reflectance of oceanic waters: accounting for Raman emission and varying particle scattering phase function. Applied Optics, 41, 6289-6306.

Navarro, G., Ruiz, J., 2006. Spatial and temporal variability of phytoplankton in the Gulf of Cádiz through remote sensing images. Deep-sea Res., II, 53, 1241-1260.

Nezlin, N.P., Lacroix, G., Kostianoy, A.G., Djenidi, S., 2004. Remotely sensed seasonal dynamics of phytoplankton in the Ligurian Sea in 1997-1999. Journal of Geophysical Research, 109, C07013, 10.1029/2000JC000628.

Oguz, T., Deshpande, A.G., Malanotte-Rizzoli, P., 2002. The role of mesoscale processes controlling biological variability in the Black Sea coastal waters: inferences from SeaWiFS-derived surface chlorophyl field. Continental Shelf Research, 22, 1477-1492.

Oguz, T., Ediger, D., 2006. Comparison of in situ and satellite-derived chlorophyll pigment concentrations, and impact of phytoplankton bloom on the suboxic layer structure in the western Black Sea during May-June 2001. Deep-Sea Research, II, 53, 1923-1933.

Oguz, T., Dippner, J.W., Kaymaz, Z., 2006. Climatic regulation of the Black Sea hydrometeorological and ecological properties at interannual-to-decadal time scales. Journal of Marine Systems, 60, 235-254.

Oguz, T., Gilbert, D., 2007. Abrupt transitions of the top-down controlled Black Sea pelagic ecosystem during 1960-2000: Evidence for regime shifts under strong fishery exploitation and nutrient enrichment modulated by climate induced variations. Deep-Sea Research, I, 54, 220-242.

Ohde, T., Siegel, H., 2001. Correction of bottom influence in ocean colour satellite images of shallow water areas of the Baltic Sea. International Journal of Remote Sensing, 22, 297-313.

O'Reilly, J.E., Maritorena, S., Siegel, D.A., O'Brien, M.C., Toole, D.A., Mitchell, B.G., Kahru, M., Chavez, F.P., Strutton, P., Cota, G.F., Hooker, S.B., McClain, C.R., Carder, K.L., Mueller-Karger, F.E., Harding, L., Magnusson, A., Phinney, D., Moore, G.F., Aiken, J., Arrigo, K.R., Letelier, R., Culver, M., 2000. Ocean color chlorophyll *a* algorithms for SeaWiFS, OC2, and OC4: Version 4. *NASA Technical Memorandum, 2000-206892, vol. 11*, Chap. 2, 9-23, Eds., S.B. Hooker, & E.R. Firestone, NASA-GSFC, Greenbelt, Maryland.

Perry, A.L., Low, P.J., Ellis, J.R., Reynolds, J., 2005. Climate change and distribution shifts in marine fishes. Science, 308, 1912-1915.

Pezzulli, S., Stephenson, D.B., Hannach, A., 2005. The variability of seasonality. Journal of Climate, 53, 71-88.

Pujol, M.-I., Larnicol, G., 2005. Mediterranean sea eddy kinetic energy variability from 11 years of altimetric data. Journal of Marine Systems, 58, 121-142.

Raateoja, M., Seppälä, J., Kuosa, H., Myrberg, K., 2005. Recent changes in trophic state of the Baltic Sea along SW coast of Finland. Ambio, 34, 188-191.

Raitsos, D.E., Reid, P.C., Lavender, S.J., Edwards, M., Richardson, A.J., 2005. Extending the SeaWiFS chlorophyll data set back 50 years in the northeast Atlantic. Geophysical Research Letters, 32, L06603, 10.1029/2005GL022484.

Rantajärvi, E., Olsonen, R., Hällfors, S., Leppänen, J.-M., Raateoja, M., 1998. Effect of sampling frequency on detection of natural variability in phytoplankton: Unattended high-frequency measurements on board ferries in the Baltic Sea. ICES Journal of Marine Science, 55, 697-704.

Reid, P.C., Edwards, M., Hunt, H.G., Warner, A.J., 1998. Phytoplankton change in the North Atlantic. Nature, 391, 546.

Robinson, A.R., McGillicuddy, D.J., Calman, J., Ducklow, H.W., Fasham, M.J.R., Hoge, F.E., Leslie, W.G., McCarthy, J.J., Podewski, S., Porter, D.L., Saure, G., Yoder, J.A., 1993. Mesoscale and upper ocean variabilities during the 1989 JGOFS bloom study. Deep-Sea Research, Part II, 40, 9-36.

Ruiz, J., Echevarría, F., Font, J., Ruiz, S., García, E., Blanco, J.M., Jiménez-Gomez, F., Prieto, L., González-Alaminos, A., García, C.M., Cipollini, P., Snaith, H., Bartual, A., Reul, A., Rodríguez, V., 2001 Surface distribution of chlorophyll, particles and gelbstoff in the Atlantic jet of the Alborán Sea: from submesoscale to subinertial scales of variability. Journal of Marine Systems, 29, 277-292.

Rydberg, L., Ærtebjeg, G., Edler, L., 2006. Fifty years of primary production measurements in the Baltic entrance region, trends and variability in relation to land-based input of nutrients. Journal of Sea Research, 56, 1-16.

Sancak, S., Besiktepe, S.T., Yilmaz, A., Lee, M., Frouin, R., 2005. Evaluation of SeaWiFS chlorophyll-a in the Black and Mediterranean Seas. International Journal of Remote Sensing, 26, 2045-2060.

Sandén, P., Håkansson, B., 1996. Long-term trends in Secchi depth in the Baltic Sea. Limnology and Oceanogr., 41, 346-351.

Santoleri, R., Banzon, V., Marullo, S., Napolitano, E., D'Ortenzio, F., Evans, R., 2003. Year-to-year variability of the phytoplankton bloom in the southern Adriatic Sea (1998-2000): Sea-viewing Wide Field-of-view Sensor observations and modeling study. Journal of Geophysical Research, 108, 8122, 10.1029/2002JC001636.

Schwarz, J.N., 2005. Derivation of dissolved organic carbon concentrations from SeaWiFS data. International Journal of Remote Sensing, 26, 283-293.

Siegel, H., Gerth, M., Ohde, T., Heene, T., 2005. Ocean colour remote sensing relevant water constituents and optical properties of the Baltic Sea. International Journal of Remote Sensing, 26, 315-330.

Siegel, H., Gerth, M., Tschersich, G., 2006. Sea surface temperature development of the Baltic Sea in the period 1990-2004. Oceanologia, 48(S), 119-131, 2006.

Shiskin, J., 1978. Seasonal adjustment of sensitive indicators. In "Seasonal Analysis of Economic Time Series", U.S. Department of Commerce, Bureau of the Census, Eds Zeller, A., pp.97-103.

Smyth, T.J., Miller, P.I., Groom, S.B., Lavender, S.J., 2001. Remote sensing of sea surface temperature and chlorophyll during Lagrangian experiments at the Iberian margin. Progress in Oceanography, 51, 269-281.

Suikkanen, S., Laamanen, M., Huttunen, M., 2007. Long-term changes in summer phytoplankton communities of the open northern Baltic Sea. Estuarine, Coastal and Shelf Science, 71, 580-592.

Tedesco, L., Socal, G., Bianchi, F., Acri, F., Veneri, D., Vichi, M., 2007. NW Adriatic Sea biogeochemical variability in the last 20 years (1986-2005). Biogeosciences, 4, 673-687.

Tilstone, G.H., Smyth, T.J., Gowen, R.J., Martinez-Vicente, V., Groom, S.B., 2005. Inherent optical properties of the Irish Sea and their effect on satellite primary production algorithms. J. Plank. Res., 27, 1127-1148.

Trzosińska, A., 1990. Seasonal fluctuations and long term trends of nutrient concentrations in the Polish zone of the Baltic Sea. Oceanologia, 29, 27-50.

Vantrepotte, V., Brunet, C., Mériaux, Lécuyer, E., Vellucci, V., Santer, R., 2007. Bio-optical properties of coastal waters in the eastern English Channel. Estuarine, Coastal and Shelf Science, 72, 201-212.

Volpe, G., Santoleri, R., Vellucci, V., Ribera d'Acalá, M., Marullo, S., D'Ortenzio, F., 2007. The colour of the Mediterranean Sea: Global versus regional bio-optical algorithms evaluation and implication for satellite chlorophyll estimates. Remote Sensing of Environment, 107, 625-638.

Wang, M., Franz, B.A., Barnes, R.A., McClain, C.R., 2001. Effects of spectral bandpass on SeaWiFS-retrieved near-surface optical properties of the ocean. Applied Optics, 40, 343-348.

Wang, M., Knobelspiesse, K.D., McClain, C.R., 2005. Study of the Sea-viewing Wide Field-of-View Sensor (SeaWiFS) aerosol optical property data over ocean in combination with the ocean color products. Journal of Geophysical Research, 110, D10S06, 10.1029/2004JD004950.

Wasmund, N., Nausch, G., Matthäus, W., 1998. Phytoplankton spring blooms in the southern Baltic Sea - Spatio-temporal development and long-term trends. Journal of Plankon Research, 20, 1099-1117.

Wasmund, N., Andrushaitis, A., Łysiak-Pastuszak, E., Müller-Karullis, B., Nausch, G., Neumann, T., Ojaveer, H., Olenina, I., Postel, L., Witek, Z., 2001. Trophic status of the south-eastern Baltic Sea: A comparison of coastal and open areas. Estuarine, Coastal and Shelf Science, 53, 849-964.

Wasmund, N., Uhlig, S., 2003. Phytoplankton trends in the Baltic Sea. ICES Journal of Marine Science, 60, 177-186.

Werdell, P.J., 2005. Ocean color K490 algorithm evaluation. http://oceancolor.gsfc.nasa.gov/REPROCESSING/SeaWiFS/R5.1/k490_update.html.

Wild-Allen, K., Lane, A., Tett, P., 2002. Phytoplankton, sediment and optical observations in Netherlands coastal water in spring. Journal of Sea Research, 47, 303-315.

Willson, R.C., and Mordvinov, A.V., 2003. Secular total solar irradiance trend during solar cycles 21-23. Geophysical Research Letters, 30, 1199, 10.1029/2002GL016038.

Yoder, J.A., Kenelly, M.A., 2003. Seasonal and ENSO variability in global ocean phytoplankton chlorophyll derived from 4 years of SeaWiFS measurements. Global Biogeochemical Cycles, 17, 1112, 10.1029/2002GB001942.

Yunev, O.A., Moncheva, S., Carstensen, J., 2005. Long-term variability of vertical chlorophyll *a* and nitrate profiles in the open Black Sea: Eutrophication and climate change. Marine Ecology Progress Series, 294, 95-107.

Yurganov, L.N., Grechko, E.I., Dzhola, A.V., 1997. Variations of carbon monoxide density in the total atmospheric column over Russia between 1970 and 1995: Upward trend and disturbances, attributed to the influence of volcanic aerosols and forest fires. Geophysical Research Letters, 24, 1231-1234.

Zibordi, G., Strömbeck, N., Mélin, F., Berthon, J.-F., 2006a. Tower based radiometric observations at a coastal site in the Baltic Proper. Estuarine, Coastal and Shelf Science, 69, 649-654.

Zibordi, G., Holben, B.N., Hooker, S.B., Mélin, F., Berthon, J.-F., Slutsker, I., Giles, D., Vandemark, D., Feng, H., Rutledge, K., Schuster, G., Al Mandoos, A., 2006b. A network for standardized ocean color validation measurements. EOS Transactions of the American Geophysical Union, 87, 30, 293, 297.

Zweifel, U.L., Wikner, J., Hagström, Å., Lundberg, E., Norrman, B., 1995. Dynamics of dissolved organic carbon in a coastal ecosystem. Limnology and Oceanography, 40, 299-305.

European Commission

EUR 23579 EN – Joint Research Centre – Institute for Environment and Sustainability
Title: Temporal Variability of Ocean Colour Derived Products in European Seas
Author(s): V. Vantrepotte & F. Mélin
Luxembourg: Office for Official Publications of the European Communities
2008 – 52 pp. – 21 x 29.7 cm
EUR – Scientific and Technical Research series – ISSN 1018-5593

Abstract
The ten-year record of ocean colour data provided by the SeaWiFS mission is an important asset for monitoring and research activities conducted on the optically-complex European seas. This study mainly makes use of the SeaWiFS data set of normalized water leaving radiances L_{WN} to study the major characteristics of temporal variability associated with optical properties across the entire European domain. Specifically, the time series of L_{WN}, band ratios, diffuse attenuation coefficient $K_d(490)$ and concentration of chlorophyll *a* Chl*a* are decomposed into terms representing a fixed seasonal cycle, irregular variations and trends, and the contribution of these components to the total variance is described for the various basins. The diversity of the European waters is fully reflected by the range of results varying with regions and wavelengths. Generally, the Mediterranean and Baltic seas appear as two end-members with, respectively, high and low contributions of the seasonal component to the total variance. The existence of linear trends affecting the satellite products is also explored for each basin. The interpretation of the trends observed for L_{WN} and band ratios is not straightforward, but it circumvents the limitations resulting from the levels of uncertainty, very variable in space and often high, that characterize derived products such as Chl*a* in European waters. Results for $K_d(490)$ and Chl*a* are also analyzed. Statistically significant, and in some cases large, trends are detected in the Atlantic Ocean west of the European western shelf, the central North Sea, the English Channel, the Black Sea, the northern Adriatic, and various regions of the Mediterranean Sea and the northern Baltic Sea, revealing changes in the concentrations of optically significant constituents in these regions.

The mission of the JRC is to provide customer-driven scientific and technical support for the conception, development, implementation and monitoring of EU policies. As a service of the European Commission, the JRC functions as a reference centre of science and technology for the Union. Close to the policy-making process, it serves the common interest of the Member States, while being independent of special interests, whether private or national.